TECHNICAL AND VOCATIONAL TRAINING INSTITUTE

(TVTI)

School of Graduate studies

FACULTY OF ELECTRICAL AND ELECTRONICS TECHNOLOGY AND INFORMATION AND COMMUNICATION TECHNOLOGY

(DEPARTMENT OF ELECTRICAL AND ELECTRONICS TECHNOLOGY)

PERFORMANCE ANALYSIS OF BACTERIAL FORAGING OPTIMIZATION ALGORITHM TUNED FRACTIONAL ORDER PROPORTIONAL INTEGRAL DERIVATIVE CONTROLLER FOR SPEED CONTROL OF PERMANENT MAGNET SYNCHRONOUS MOTOR

MSc Thesis for the Partial Fulfillment of

Master of Science in Electrical Automation and Control Technology Management

By,

HENOK NEGASH SEIFU(MTR/603/13)

Supervisor,

Dr. DEREJE SHIFERAW

January, 2023

Addis Ababa, Ethiopia

Performance Analysis of Bacterial Foraging Optimization Algorithm tuned Fractional order Proportional Integral Derivative controller for Speed control of Permanent Magnet Synchronous Motor

A Thesis paper submitted to

TECHNICAL AND VOCATIONAL TRAINING INSTITUTE

(TVTI)

FACULTY OF ELECTRICAL AND ELECTRONICS TECHNOLOGY AND INFORMATION AND COMMUNICATION TECHNOLOGY

(DEPARTMENT OF ELECTRICAL AND ELECTRONICS TECHNOLOGY)

In partial fulfillment for the Degree

MASTER OF SCIENCE IN ELECTRICAL AUTOMATION AND CONTROL TECHNOLOGY MANAGEMENT

By,

HENOK NEGASH (MTR/603/13)

Supervisor,

Dr. DEREJE SHIFERAW

DECLARATION

I hereby affirm that the work being presented in this thesis, “Performance analysis of Bacterial Foraging Optimization Algorithm tuned Fractional order Proportional Integral Derivative controller for Speed control of Permanent Magnet Synchronous Motor" is entirely my own original work, hasn't been submitted for credit at this or any other university, and has correctly cited all relevant sources.

NAME HENOK NEGASH (MTR/603/13)

signature_____

Location: Addis Ababa

Submission date: _____

In my capacity as a university advisor, I have given permission for this thesis to be submitted for review.

Dr. DEREJE SHIFERAW (Associate prof.)		05/01/2023
Advisor Name	Signature	Date

TECHNICAL AND VOCATIONAL TRAINING INSTITUTE (TVTI)

FACULTY OF ELECTRICAL AND ELECTRONICS TECHNOLOGY AND INFORMATION AND COMMUNICATION TECHNOLOGY
(DEPARTMENT OF ELECTRICAL AND ELECTRONICS TECHNOLOGY)

Thesis on

Performance Analysis of Bacterial Foraging Optimization Algorithm tuned Fractional order Proportional Integral Derivative controller for Speed control of Permanent Magnet Synchronous Motor

By,

HENOK NEGASH (MTR/603/13)

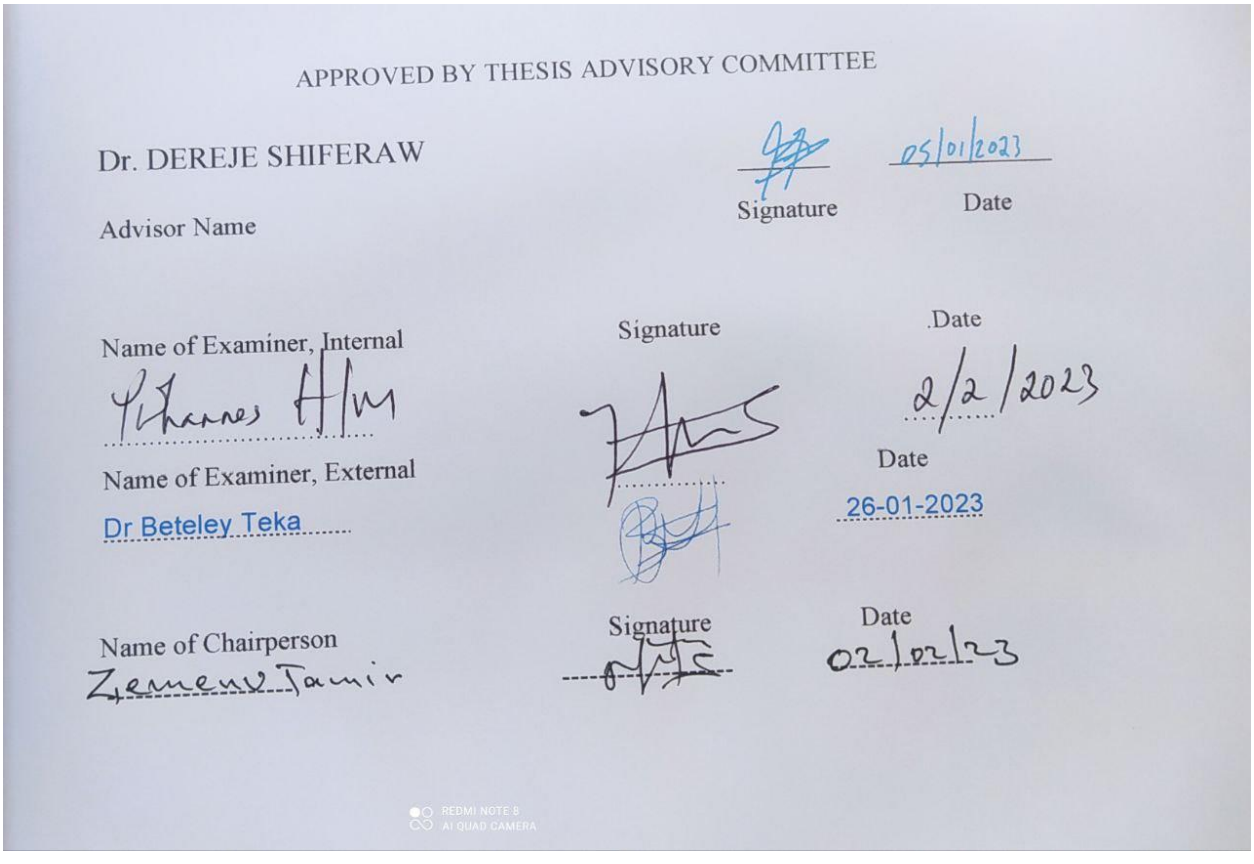

APPROVED BY THESIS ADVISORY COMMITTEE

Dr. DEREJE SHIFERAW — Signature — 05/01/2023 Date

Advisor Name

Name of Examiner, Internal — Signature — .Date

Yihannes H/M — 2/2/2023

Name of Examiner, External — Date

Dr Beteley Teka — 26-01-2023

Name of Chairperson — Signature — Date

Zemenu Tamir — 02/02/23

ACKNOWLEDGEMENT

I want to start by giving glory to the mighty God who has helped me throughout my entire life through a number of people, including academic and supportive staff from the Electrical and Electronic department. I also want to acknowledge and thank my closest friends as well as my family and relatives who helped me with my thesis both directly and indirectly while I was a graduate student. Additionally, I will always be thankful to my adviser, Dr. DEREJE SHIFERAW, for her counsel and direction, which have been helpful. Additionally, I want to thank all of my friends and classmates who provided me with directions.

ABSTRACT

Multi-phase Synchronous Motor is a popular industrial application because of its excellent dependability, low cost, and low maintenance needs. It takes less time to develop a vector controller to control the magnitude and phase quantities of PMSM. The stator voltage vector is only controlled in amplitude and frequency using the vector control approach, which ignores the position of the rotor. The purpose of this thesis is to determine which method produces the best results. PID-operating PMSM the controller is simply turned and manages the system by tweaking it using MATLAB/Simulink software tools to change the load torque parameter modification and bacteria algorism. Bacterial algorism using simulation results shows a fractional order PID controller for permanent magnet synchronous motor based on a technique that implements fractional order differential operation. When comparing the settling times , rise times and overshot of the speed control of PMSM for the PID and the FOPID controller based BFO tuning, the FOPID controller has reduced the settling times, rise times, and overshoot by 72.6%,85.6% and 88.3% respectively. It can be seen that the FOPID controller significantly increased the system's efficiency and performance.

Keywords: Permanent magnet synchronous motor **(**PMSM), Proportional integral derivative (PID), Bacterial forging optimal algorism (BFOA)

Table of Contents

List of Figure

List of Table

Abbreviations

AC …….	Alternating Current
DC ……	Direct Current
EMF ……	Electro Motive Force
FLC ……..	Fuzzy Logic Controller
FOC …….	Filed Oriented Control
mmf …….....	magneto motive force
PI…….....	Proportional Integral
PID…….	Proportional Integral Derivative
PM…….	Permanent Magnet
PMSM……	Permanent Magnet Synchronous motor
PWM……..	Pulse width modulation
SPMSM……..	Surface Mount permanent magnet synchronous motor
SVMPWM……..	Space vector pulse width modulation
VSI…….	Voltage source inverter
i_{qs_ref}	Reference q axis synchronous current
i_{ds_ref}	Reference d axis synchronous current
iqs.....	q -axis synchronous current
iqs.....	d -axis synchronous

.

CHAPTER ONE
INTRODUCTION

1.1 Background

As opposed to electromagnets, permanent magnets implanted on the rotor are used in permanent magnet synchronous motors (PMSM) to produce the air gap magnetic field. As the magnetic field rotates at synchronous speed, permanent magnets on the rotor poles magnetically pair with it. A number of advantages, These motors' use of permanent magnets instead of rotor windings results in their great efficiency, high power density, zero copper loss, quick dynamic response, robustness, and electrical stability[1]. Due to these significant benefits, PMSMs are used in hybrid electric vehicles, electric vehicles, industrial motors, elevators, escalators, computer peripheral devices, robotics, and other devices, among others. Using multiphase machines results in fewer torque ripples, higher torque per phase current, and a dependable drive that keeps running even if one or more phases fail when compared to three-phase machines. Due to these benefits, multiphase machines have drawn more attention from academics who are interested in using them in crucial applications such ship propulsion systems, offshore wind farms, and electric airplanes. The most popular multiphase machines are the synchronous or multiphase induction machines. In this study, the multi-phase permanent magnet synchronous motor drive will receive specific attention (PMSM).The literature has recommended a number of control strategies to enable an efficient control of multi-phase PMSM. These control strategies all result in decoupled control between flux and torque, much like a DC machine with distinct excitation, although having different underlying philosophies. One of these strategies is the precise regulation of torque. It has straightforward control architecture because it doesn't need internal current control loops, a pulse width modulation block, or a lot of parameter dependence, which results in better dynamic performance than vector control. Hysteresis controllers are used, but they produce variable switching frequencies, which cause high waves to appear in the torque and stator flux. The primary issue with the traditional DTC is this latter flaw.

1.2 Problem Statement

Since, PMSM has seen a rise in use in high-performance applications like robotics and industrial

machines, which call for speed controllers that offer not only precision and great performance but also flexibility and efficiency in the design and implementation processes. The performance quality of the pre-design of the motor driving system is constantly lowered by the numerous uncertainties present in industrial applications, such as system parameter uncertainty, external load disturbance, friction force, and unmolded uncertainty. By using PID and FOPID the performance of the system is not better than BFO tuning technique. So the main aim of this study is to improve the performance of PMSM by using PID and FOPID controller with BFO tuning technique

1.3 OBJECTIVES

1.3.1 General objectives

- The main aim of this thesis is to perform a comparative analysis of PID and Fractional order PID-tuned with Bacterial Foraging Optimization (BFO) for speed control of PMSM.

1.3.2 Specific objectives

- To design both PID and FOPID controller for speed control of PMSM
- To implement the proposed PID and FOPID controller tuned with BFO in MATLAB/Simulink
- Compare PID and FOPID Optimized by BFO based on the outcomes of their output simulations

1.4 Scope and limitation

Various techniques are employed. In this instance, BFOA-based algorithms were utilized to simulate MATLAB/Simulink and provide great dynamic performance. To the extent that the researcher's work was restricted to the BFOA regulation of PMSM, the overall general objective and specific objectives must be fulfilled.

1.5 Organization of the Thesis

This thesis includes five chapters. The first chapter generally presents the introduction of the speed control of PMSM using PID and FOPID controller tuned by BFO techniques which is the

background of the PMSM speed control, statement of the problem, relevance, objectives of the study, methodology, scope and limitation of the study are present in this chapter. Different literatures, related to speed control of PMSMs, are reviewed in chapter two. In chapter three, it presents the different control theory techniques of the PMSM. System modeling, designing, analysis and implementation are presented in chapter four. Simulation results are presented and discussed in chapter five. The contributions of the thesis work are also discussed in the same chapter. Finally, chapter six presents conclusions and recommendations.

1.6 Methodology

This thesis proceeds through different phases starting from the beginning of the work up to the final report of the designing and simulation of speed control of PMSM drive. Maintaining the whole process is quite important to minimize the probability of the problem happening during the work.

- The first task is organizing the literature reviews where all the theoretical information regarding the PMSM drive to be gathered from and a comparison of previous similar research papers have been discussed.
- The characteristics and mathematical modeling of PMSM drive theory have been studied
- Based on mathematical model of the PMSM drive, a PID and FOPID controller tuned by BFO have been developed.
- Then, speed control of PMSM using a PID and FOPID controller tuned by BFO have been simulated by MATLAB/Simulink.

CHAPTER TWO
LITERATURE REVIEW

2.1 Introduction

Energy conservation is given a high emphasis in many industrial applications nowadays. Induction machines (IMs) have been replaced because permanent magnet synchronous motors (PMSMs) provide a higher power density and efficiency. Additionally, there are a lot more inverter-fed PMSM drives on the market right now that use both vector and scalar control techniques. Scalar control performs worse than vector control in terms of responsiveness, system effectiveness, and other measures. However, because it ensures a straightforward control design, a low-cost implementation, and simple commissioning by the end user, the scalar control technique is utilized in many applications that do not require significant dynamic performance, such as pumps and fans [3].

Because they have smaller rotor losses, PMSM motors are becoming more and more popular. The key difference between a PMSM and an asynchronous induction motor is that the PMSM must be driven and requires an additional DC power source. The driver frequently increases the price and restricts the use of PMSM motors to high performance applications[4]. In terms of responsiveness, system effectiveness, and other metrics, scalar control performs worse than vector control. The scalar control approach is used in many applications that do not require considerable dynamic performance, such as pumps and fans, since it guarantees a simple control design, a low-cost implementation, and simple commissioning by the end user [3]. Permanent magnets on the rotor poles magnetically couple with the revolving magnetic field at synchronous speed. These motors have a number of benefits due to the use of permanent magnets as the rotor windings, including high efficiency, high power density, no copper loss, quick dynamic response, robustness, and electrical stability [5]. PI or PID controllers are widely used to control PMSM speed. The proportional-integral derivative (PID) controller is often used to govern PMSM systems in industrial applications due to its simplicity, high reliability, and efficiency[5] .Second edition, American Instrument Society, 1995. As a result, PID controller performance may suffer greatly from parameter variations. The adaptive PID speed control approach for permanent magnet synchronous motor drives can be used to address these problems [6].

Researchers have created proportional-integrator and derivative controllers, as depicted schematically. The d and q currents need the proper coefficients kp, ki, and kd to achieve the system's optimal steady state and transient response. Uncertainty, temporal variation, nonlinearity, and fractional order are characteristics of PMSM servo systems. To achieve the required control effect, the conventional control approach must be used. Due to its nonlinear nature, fuzzy control is incredibly adaptable to changing parameter values and inaccurate representations of the controlled object. Three closed-loop simulation models for permanent magnet synchronous motors are developed. A vector control approach is used to examine the control theory and application of space vector pulse width modulation (SVPWM). The proportional integral differential (PID) controller's parameters may be self-tuned using an algorithm thanks to the motor's fractional-order feature. The controller is chosen to control the servo motor's position. It combines the adaptability of algorithm control with the accuracy of a fractional-order PID controller and employs feed-forward to accelerate reaction time. The outcomes show how well the control system works and how well it can fulfill the requirements for servo control in trajectory tracking. The route tracking research used several unique pathways. Utilizing the speed and position tracking test of the PMSM AC servo system on the test verification platform, the performance of the control algorithm is assessed. [8]. A new base extended state observer may be used. The first example shows a completely new PID sliding mode surface with nonlinear differential, integral, and proportional terms. In the second item, a unique compound control method based on an extended state observer is shown. Then, using the unique sliding surface, a distinct super-twisted fractional-order PID sliding mode of the PMSM is constructed. The usage of adaptive super-twisting nonlinear fractional-order PID sliding mode contortion is therefore advised for the PMSM. The comparison's outcomes are then displayed [9] .Use the fractional order PID controller approach of parameter modifying along with the bacterial foraging optimization algorithm in Simulink for increased controller performance. There are several advantages to synchronizing motors with constant volts per hertz in an open loop. The supply voltage's frequency may be utilized to determine the angular speed. If the external load torque is less than the break load torque, the angular speed produced under that assumption is taken to be the rotor's valve speed. It takes less time to implement the control magnitude and phase quantities of a scalar controller for a PMSM. Without taking into account the location of the rotor, scalar control just controls the amplitude and frequency of the stator

voltage vector. Finding the tactic that will result in the best results is the aim of this thesis. PID controllers include speed controllers that fall under a different category. The most straightforward approach to administering a PMSM is scalar control. As a result, across the whole range of motor speeds, the connection between voltage (current) and frequency holds true. To maintain their ratio constant, the voltage (current) amplitude and frequency are changed in accordance with the required synchronous speed. Scalar control replicates the impact of load torque on speed as contrasted to meaningless control since speed varies when torque is lowered and when speed reaches its controlled pace. The PSO algorithm, a well-known optimization method, is based on the social organization of animals like fish schools and bird flocks. A number of particles donate a collection of optimization particles in a multidimensional search space that search for the optimal solution. This approach establishes the most optimized value for each particle by convergence [10]. One of the essential components of a mini quad is an AC motor. Every autonomous function of the little quadcopter requires its powerful AC motor. It must thus function better because of this. Designing gasoline motors for use in airplanes with exceptional energy efficiency might be one approach. Another tactic is to run machinery correctly. Tailor-made quadcopters use variable speeds for a number of tasks. Variable speed drives and adjustable speed drives are phrases used in literature to refer to devices that alter an electrical machine's speed to regulate functioning. These three components will each be covered separately [11].

The PMSM is more effective and has a greater torque-to-weight ratio than the inverter-fed induction motor drive because it has no rotor loss. However, a critical shortcoming of the conventional PMSM is the requirement for correct management of the inverter switches in order to employ a rotor position sensor, such as a high-resolution encoder. In order to reduce costs and improve dependability, sensor-less PMSM control systems have been developed. For closed-loop speed control, these methods employ an estimated motor position and speed as a feedback signal [13].

2.2 AC Motors

UAVs use AC motors with exceptional performance, particularly for small quadcopters, as a result of their success in motion control and the expansion of their use. In order to satisfy

different objectives, it is crucial to select the proper control algorithms for AC motors in tiny quadcopters. Due to the extreme differences in their operating theories, physical characteristics, and levels of power, there are numerous different types of these devices. Based on their underlying working concepts, synchronous and induction motors are the two fundamental subcategories into which AC motors are frequently subdivided. There are two variations of each type of motor[13].Pulse width modulation has been the subject of extensive research over the last few decades (PWM). Numerous PWM approaches have been successful in achieving the following goals. There are several benefits including a large linear modulation range, reduced switching loss and total harmonic distortion (THD) in the switching waveform's spectrum, easy implementation, and quick computation times[13].Space vector modulation is a technique used to control pulse width modulation. The most common alternating current waveform for driving three-phase AC motors at various speeds is created using it. Space vector pulse width modulation uses a switching frequency that is constant. This makes it possible to easily alter the switching frequency [14]. Since significant advancements in the particular machine control methods have been made, every industrial application can operate well with the right supplying-motor assembly [15]. Other names for vector control are field-oriented control or control of vectors decoupling. Thus, flux and torque may be directly controlled. The PMSM can therefore be converted into a separately stimulated dc machine by employing vector control. The PMSM model is nonlinear. Consequently, the model of PMSM is linear and uses vector control[16].

Permanent magnet synchronous motor types and fundamental construction Permanent magnet synchronous motors can be classified as convex type, embedded type, and various varieties depending on the rotor configuration. The first two are referred to as the external constructions when they are combined. The convex type has the benefits of a straightforward structure, a low cost, and a variety of uses. The motor's rotor is frequently utilized in servo systems because of its small diameter and low moment of inertia. The flux leakage coupling can be strengthened by the embedded structure, resulting in a larger pole angle and less torque. Despite having a more complex structure and costing more than a built-in motor, it is better suited for use in high torque situations because it can generate more torque than a convex motor thanks to its larger air gap flux density. A permanent magnet synchronous motor's stator, end cover, and other parts. Outstanding permanent magnet poles on the rotor set it apart from asynchronous motors. It may

also be known as surface rotor structure or built-in rotor structure depending on where the permanent magnets are located on the rotor[18].

2.3 Characteristics of PMSM

Low Loss and Low Rise in Temperature When compared to magnetic fields produced by excitation current, permanent magnets provide the magnetic field, preventing excitation loss and lowering the motor's temperature rise. The temperature increase may lowered by more than 20K while still carrying the same load. High power factor and effective energy conservation A permanent magnet synchronous motor has a high power factor that is unaffected by motor stage. The power factor is close to one when the load is at maximum capacity. In this reason, this is more efficient than an asynchronous motor. Theoretically, a high power factor allows a motor's power supply (transformer) capacity to be decreased while simultaneously lowering the requirements for supporting switchgear and cables[18]. Permanent magnet synchronous motor drive system The four core components of the motor drive are the PMSM, inverter, primary control unit, and position sensor. ties that connect the components[19].

2.4 PID controller tuning methods

Traditional techniques for modifying PID parameters
For well-known models, this family of tuning techniques seeks to provide controller configurations. System dynamics are calculated using step responses (Bansal etal., 2012). Different equations that describe this response have given rise to a number of conventional methods. Despite the fact that traditional PID tuning methods are frequently employed, their behaviors typically deviate from the desired objective or goal (Reis et al., 2016).

Ziegler and Nichols published the initial description of the tuning method in 1942, which is still widely accepted and used today (ström and Hägglund, 2004). With the use of the transient step reaction, Ziegler and Nichols did a significant amount of study and created standards for figuring out a plant's KP, KI, and KD values. There were supplied both closed-loop and open-loop methods. Process gain (KP), process time constant (Tp), and process dead time are the key process parameters that may be obtained utilizing the ZN tuning approach (Lp).

Ziegler and Nichols created and published the Ziegler-Nichols tuning technique in 1942 (ström and Hägglund, 2004). It is still often used nowadays. Based on their findings and recommendations, Ziegler and Nichols determined the KP, KI, and KD values for a plant's transient step reaction. Both closed-loop and open-loop techniques were offered. The main process parameters that may be acquired by using the ZN tuning method are process gain (KP), process time constant (*Tp),* and process dead time (*Lp).* Ziegler and Nichols suggested utilizing various criteria for closed and open loops depending on the values of KP, TI, and TD. Gain and Phase Method: In comparison to the ZN test, ström and Hägglund (1984) developed a test that was much simpler to carry out in automated loop tuners. Instead of changing proportional gain, they advocated relay nonlinearity as the nonlinear function. A gain and phase approach for the detection of some Nyquist curve locations was presented by ström and Hägglund (1984) in order to get around the "trail by accident" restriction of the Z-N methodology. where m stands for the projected phase margin and Am for the ideal gain margin. How near the (1 + j0) point a control system's polar plot is may be seen in the phase and gain margins [20].

When setpoint monitoring and disturbance rejection are necessary, a variety of industrial applications often employ PID controllersThis controller delivers optimal and dependable performance for stable, unstable, and nonlinear systems under a variety of operating situations. The PID is divided into three classes based on the controller configuration: ideal PID, series PID, and parallel PID (position of P, I, and D) [21]. Multi-phase and multi-level inverter technologies have become well known as a practical technique to get past the current and voltage restrictions of power switching converters in the context of high-power, medium-voltage drive systems. Particularly when compared to conventional three-phase motor drives, multi-phase motor drives provide a number of advantages, such as the ability to reduce the amplitude and frequency of torque pulsations while improving rotor harmonic current losses and dc link harmonics. Due to its redundant design, multiphase motor drives further improve system dependability[22] .Scientific studies on fractional-order controllers in general, with a concentration on the fractional order PID, have increased significantly during the past few years. This controller has been made available in a variety of configurations with a range of tweaking methods and implementation choices. The practical usage of such controllers has been covered in a number of recent studies. However, it will be a while before these controllers are accepted by industry. Such

fractional order PIDs may become more and more suitable for industrial applications as a result of auto tuning techniques. The various auto-tuning techniques for PIDs with fractional orders are examined in this work. The most recent findings are the main focus. For various processes, a comparison of a number of auto tuning strategies is taken into account. Numerical examples are provided to illustrate the concepts' applicability to basic industrial processes [23].

2.5 Summary of Literature Review

In this thesis, after the analysis review and comparison of several speed control PMSM techniques performance analysis of bacterial foraging optimization algorithm tuned fractional order proportional integral derivative controller for speed control of permanent magnet synchronous motor used.

Speed control of PMSM drives has been a topic of interest for the new invented technology .the vector control, fractional order proportional integral derivative controller, and Traditional techniques for modifying PID parameters.

This paper compares the speed response of proposed controlled in general performance analysis of bacterial foraging optimization algorithm tuned fractional order proportional integral derivative controller for speed control of permanent magnet synchronous motor by using speed ,load and without load ,parameter variation.

CHAPTER THREE

MATHEMATICAL MODELLING OF A SPEED CONTROL OF PMSM

3.1 Introduction

The term "electric drive systems" is where the idea of controlling an AC motor primarily arises. Drives operate and regulate the direction, speed, and torque of moving things. Drives are frequently employed in applications involving speed control or motion. Electric motors are controlled by specific drives known as electrical drives. Drives come in both continuous and variable forms Because constant speed motors are useless for operations requiring varying speeds In these situations, Using variable speed drives, , a wide variety of speeds are used to move the weights [24].

Due to its superiority over competing motors in the majority of industries, AC drives are used to drive AC motors, particularly three phase induction and synchronous motors. The phrases variable frequency drive (VFD), variable speed drive (VSD), and adjustable speed drive are also used in the industrial sector (ASD). A fixed input voltage and frequency are converted into a variable output voltage and frequency by all forms of AC drives, despite the fact that there are multiple different types. The motor's speed is controlled by the drive's frequency, and the voltage and frequency of operation define how much torque the motor is capable of producing [24].

3.2 AC Motor Control Strategies

Switching in different numbers of poles had an impact on previous speed controllers, and the only accessible control methods were rough steps that could be made manually. Modern electronic inverters, however, enable constantly changeable frequency supply, allowing closed loop speed control. Numerous speed control strategies are employed for AC motor control schemes that use variable frequency drives. Figure 3.1 displays the specific categories of AC motor control systems. Scalar and vector control systems make up the majority of the control methods utilized in current AC drive systems. These are explanations of certain methods [25].

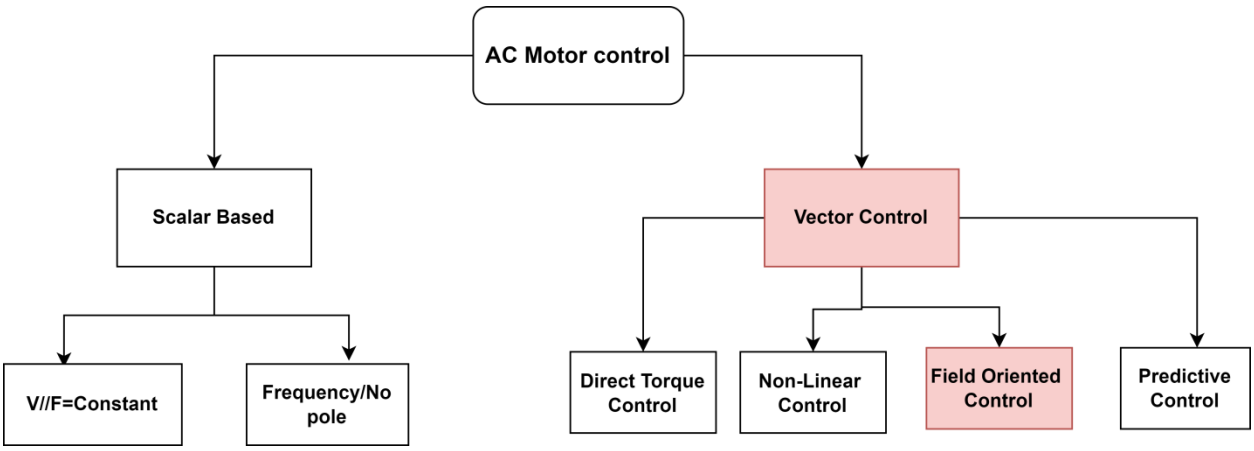

Figure 3.1 : Classification of AC motor controls

3.2.1 Scalar Control Method

One of the simplest methods for controlling PMSMs is a scalar V/f (voltage/frequency) control system Depending on the motor's speed range it maintains a constant relationship between current or voltage and frequency. In this open loop control strategy, the characteristics or location of the motor are not taken into consideration[25]. As a result, the hardware control uses less computational power, and if a certain applied frequency is surpassed, the drive system becomes unstable. For frequency synchronization, damper windings have been included into the PMSM rotor. For a five-phase PMSM, an open-loop V/f stabilizing approach is provided in [25] that maintains the drive system's stability throughout a large speed range. Two feedback adjustments are made to the V/f control to keep the stator's supplied frequency at a consistent level: I I use active power fluctuation to alter the speed stabilizing factor, and I use PI regulation of the q-axis current component to control the voltage amplitude and achieve unity power factor.

3.2.2 Vector Control Methods

Vector approaches were created to overcome the problems with scalar control methods starting in the 1970s [25]. The high level of control of AC drives has also been revived as a result of the finding that synchronous motors may be controlled similarly to individually exited DC motors.

This control system enables the amplitude, frequency, and angle of the supplied voltages to be changed. It suggests that it is possible to predict the size and direction of the space vectors.

Vector control is methods for making a machine behave like a DC motor that has been individually evacuated. It is sometimes referred to as vector control, orthogonal control, and decoupling. Both synchronous and induction motor drives can use vector control [26] [27] and [28].

The Filed oriented control mechanism is one of the several vector control techniques applied in this study. As a result, the mathematical model and FOC control mechanism of the PMSMs are also covered in the next section. By applying inverse transformations, such as Park and Clarke's, this can be demonstrated using space vector theory. The final sentence describes the dynamics employed in the PMSM drive [25].

3.3 Field Oriented Control (FOC)

The amplitude and phase of the stator current and voltage for each phase are controlled by electrical drives based on the vector control (FOC) principle. Using song projections, this control converts a three-phase, speed-dependent system into a two-coordinate, time-invariant system (d and q). These projections result in a structure that looks like a DC machine control. The PMSM must act like a DC motor for the control to work, hence it must be constantly aware of the rotor flux or position [29] [30].

This orthogonal connection prevents the armature current from affecting the field flow. As a result, there is no longer a coupling between the field flux and the armature mmf [25].

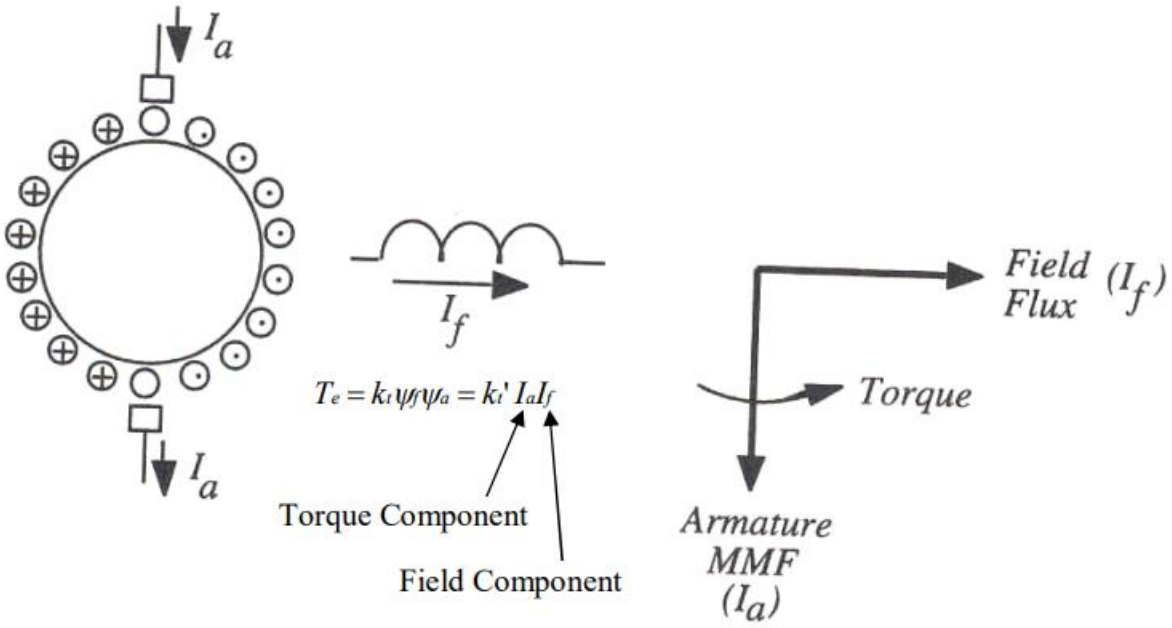

Figure 3-2: Separately excited DC Motor [26].

In order to manage the current that creates torque differently from the current that produces magnetic flux and to approximate the responsiveness of a DC motor, To quickly manage power, a field-oriented control architecture is utilized. The control is accurate in all working processes because it is independent of the mathematical model, which has a limited bandwidth (steady state and transient). For field-oriented controlled devices, the flux component and the torque element (related to the q-coordinate) are two constants that must be used as input references (associated with d- coordinate). The FOC thereby addresses the drawbacks of the conventional system in the methods listed below [26]. The FOC resolves the conventional scheme difficulties

- The simplicity of obtaining a reliable reference (torque and flux component of the stator current)
- Direct electromagnetic torque application is simple, and T_{em} control in the (d, q) reference frame.

$$T_{em} = \frac{3}{2} P \psi_m i_q \tag{3.1}$$

Where P is the pole pair, ψ_m is the permanent magnet flux linkage, and i_q is the quadrature axis current, T_{em} is the generated electromagnetic torque.

3.4 Space Vector transformation

Taking into account that the FOC comprises managing the stator currents represented by vectors. This projection-based control converts a three-phase, time- and speed-dependent system into a two-coordinate, time-invariant system (d and q co-ordinates). Assume that the three phase supply voltage matches that of the SPMSM model and that the conversions will be carried out as usual [25].The flux linkage distribution's spatial harmonics are ignored

- Deep bar effects and slot harmonics aren't taken into account
- Saturation is ignored
- Linear behavior is the norm for permanent magnets
- The neutral point is separate.
- It is believed that rotor flux is fixed at a specific operational point.
- There are very few machine core losses.
- The flux is altered by rotor temperature, however it is expected that the change over time is negligible.
- There are no dynamics of the field currents.

Rotor reference frame was chosen since stator voltages, currents, induced EMF, and torque are all individually determined by rotor position. The rotor and spinning stator field rotate at the same rate, as does the d-q coordinate system. The d-axis, which in modeling stands in for the magnetic axis of the rotor, is in fixed phase with the d-q axis of the stator. shown in Figure 3.2 as follows:

$$\vec{i}_s = i_a + \alpha i_b + \alpha^2 i_c \qquad 3.2$$

Where the spatial operators are represented by $\alpha = e^{j\frac{2}{3}\pi}$ and $\alpha^2 = e^{j\frac{4}{3}\pi}$. The complex space vector of the stator is depicted in the following figure:

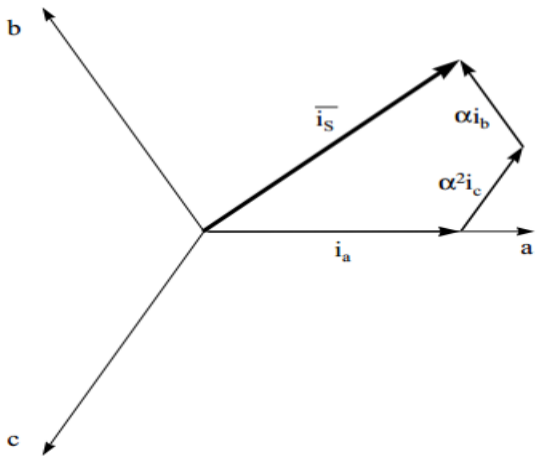

Figure 3.3: the axis-dependent element of the stator current space vector [22]

This is represented by this current space vector. Two time-invariant reference frames must be created from it. Figure 3.3 indicates that there are two fundamental processes in this transformation.

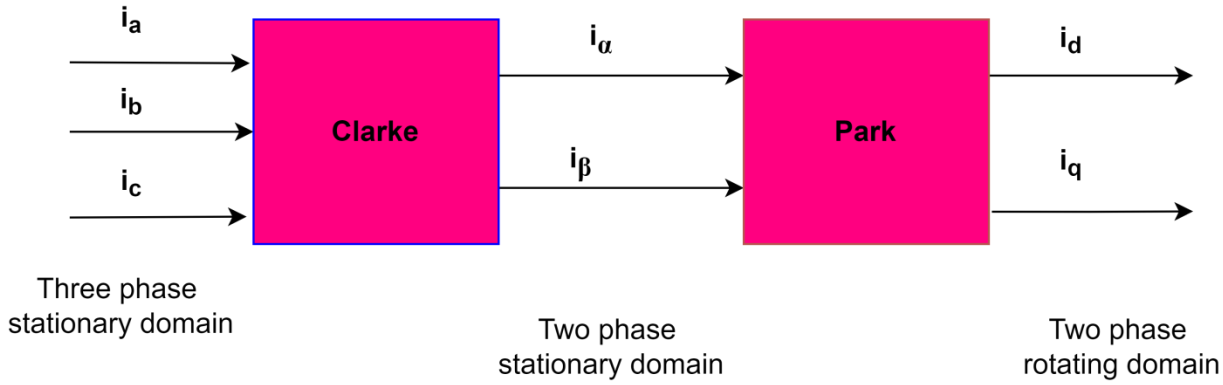

Figure 3.4: conversions from stationary three-phase frames to rotating two-phase frames

3.4.1 Clark Transformation (a, b, c) to (α, β) coordinates

With just two (α, β) orthogonal axes, the space vector may be represented in a different reference frame. In Figure 3.4[25], the following vector diagram is displayed. Assuming that the axes "a" and " α " are pointing in the same directions.

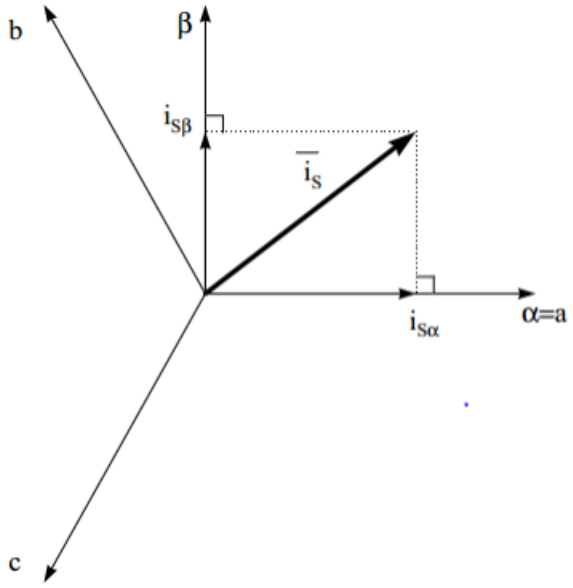

Figure 3.5: Components of the stator current space vector in the stationary reference frame [22]

The space vector may be expressed in an alternative coordinate system with only two (α, β) orthogonal axes. The following vector diagram is shown in Figure 3.4[25] in the hypothetical situation when the axes "a" and " **α** " are parallel to one another.

$$\begin{bmatrix} i_{s\alpha} \\ i_{s\beta} \end{bmatrix} = \frac{2}{3} \begin{bmatrix} 1 & -\frac{1}{2} & -\frac{1}{2} \\ 0 & \frac{\sqrt{3}}{2} & -\frac{\sqrt{3}}{2} \end{bmatrix} \begin{bmatrix} i_a \\ i_b \\ i_c \end{bmatrix} \tag{3.3}$$

3.4.2 Transformation of Park (α, β) to (d, q) coordinates

The FOC's biggest transformation is this one. The system (α, β) in the rotating reference frame d, q is really modified by this projection. The link between the current vector and the two-reference

frame is shown in Figure 3.5 below [25]. when the electrical rotor flux and d axis are coupled. where the symbol _re designates the position of the electrical rotor flow.

$$\theta_{re} = p\theta_r \tag{3.4}$$

Where p denotes how many pole pairs there are and θr denotes the rotor position, which is determined by the angle formed by the field produced by the phase "a" winding and the permanent magnets.

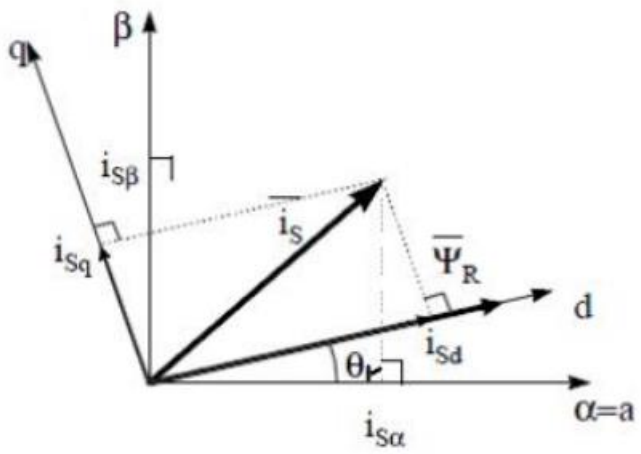

Figure 3.6: component in the rotating reference frame (d, q) [22]

The following equations *[25] are used to calculate the current vector's flux and torque components:*

$$\begin{bmatrix} i_{sd} \\ i_{sq} \end{bmatrix} = \begin{bmatrix} \cos\theta_{re} & \sin\theta_{re} \\ -\sin\theta_{re} & \cos\theta_{re} \end{bmatrix} \begin{bmatrix} i_{s\alpha} \\ i_{s\beta} \end{bmatrix} \tag{3.5}$$

v_{sd} and v_{sq} voltages are also converted to $v_{s\alpha}$ and $v_{s\beta}$ voltages using the inverse Park transformation [25]

$$\begin{bmatrix} v_{s\alpha} \\ v_{s\beta} \end{bmatrix} = \begin{bmatrix} cos\theta_{re} & -sin\theta_{re} \\ sin\theta_{re} & cos\theta_{re} \end{bmatrix} \begin{bmatrix} v_{sd} \\ v_{sq} \end{bmatrix} \tag{3.6}$$

Using the following equations [54], the three-phase stator reference frame is changed from the two-axis orthogonal reference frame.

$$\begin{bmatrix} v_{sa} \\ v_{sb} \\ v_{sc} \end{bmatrix} = \begin{bmatrix} 1 & 0 \\ -\frac{1}{2} & \frac{\sqrt{3}}{2} \\ -\frac{1}{2} & -\frac{\sqrt{3}}{2} \end{bmatrix} \begin{bmatrix} v_{s\alpha} \\ v_{s\beta} \end{bmatrix} \tag{3.7}$$

3.5 Mathematical modeling of PMSM

Only the absence of damper windings and the use of a PM rather than a field winding as The PMSM may be distinguished from a typical wound rotor synchronous machine by its excitation source.

The principle of rotating transformation is used to significantly simplify the electrical equations in the following calculation. The stator winding's two axis voltage formulae for an IPMSM are given below (they are also applicable to SPMSMs if L_d and L_q use the same value).

The total of the resistive voltage drops is used to compute the d- and q-axes stator voltages and [31] the derivative of the flux connections in the corresponding windings;

$$V_q = R_s i_q + \frac{d}{dt}(\psi_q) + \omega_{re}\psi_d \tag{3.8}$$

$$V_d = R_s i_d + \frac{d}{dt}(\psi_d) - \omega_{re}\psi_q \tag{3.9}$$

$$\psi_d = L_d i_d + \psi_m \;\; And \quad \psi_q = L_q i_q \tag{3.10}$$

where the (d, q) axis stator voltages are denoted by V d and V q, and the (d, q) axis stator currents are denoted by i d and i q. The electrical angular velocity of the rotor is represented by _re, and the d, q axis inductances are L d and L q. ψ_m is the flux linkage caused by the rotor magnets connecting the stator. The (d, q) axis stator flux linkages are ψ_d and ψ_q. R_s is the resistance of the stator windings.

Equations (3.8) and (3.9) can each be changed to Equation (3.10) to provide a more useful equation:

$$V_q = (R_s + L_q \frac{d}{dt}) i_q + \omega_{re} L_d i_d + \omega_r \psi_m \tag{3.11}$$

$$V_d = (R_s + L_d \frac{d}{dt}) i_d - \omega_{re} L_q i_q \tag{3.12}$$

Figure 3.6 depicts the stator q and d-axis coordinates. the analogous circuit of the PMSM can be determined from the dynamic Equations (3.8) and (3.9).

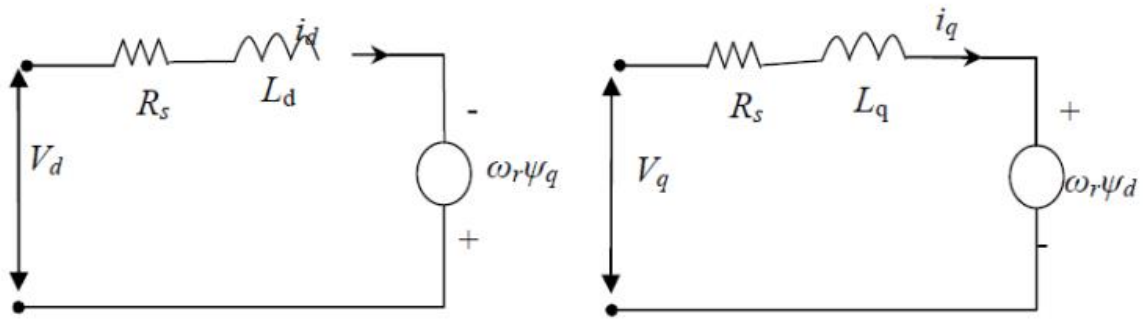

Figure 3.7: Analogous circuits for the PMSM dynamic model

(a) Circuit of the d-axis b) circuit of the q- axis

3.5.1 Equation for Electromagnetic Torque

This has the most significant influence on , which includes the positioning of the rotor as well as its rotational speed. For the purpose of calculating the electromagnetic torque, the following equation should be used [32]. When electromagnetic torque and mechanical rotor speed are brought together, it is possible to create power that may be used for mechanical applications. It is possible to determine the air gap torque by making use of the rotor speed, which is represented by the symbol _r and is supplied in mechanical rad/s. This is shown to be the case in [32] T_{em}.

$$P_m = \omega_{re} T_{em} = \frac{3}{2} \omega_r (\psi_d i_q - \psi_q i_d) \tag{3.13}$$

Mechanical speed is correlated with rotor or electrical speed as

$$\omega_r = \omega_{re} = \omega_m P \tag{3.14}$$

In this equation, P_m stands for output mechanical power, ω_m for the rotor shaft's mechanical angular velocity, ω_{re} for the electrical angular velocity of the rotor, T_{em} for the electromagnetic torque that was produced, and P for the number of pole pairs.

Equation (3.13) will provide [13] when Equations (3.10) and (3.14) are substituted.

$$T_{em} = \frac{3}{2} P\left[\psi_m i_q + \left(L_d - L_q\right) i_q i_d\right] \tag{3.15}$$

The first term in Equation (3.15) is referred to as "mutual response torque" and describes the interaction between i_q and the permanent magnet. The second term in the equation is referred to as "reluctance torque" and describes the significance.

The surface-mounted PMSM motor used in this work suggests that L d=L q=L ds denotes that the "reluctance torque" is equal to zero. The torque statement for SPMSM is therefore [31]:

$$T_{em} = \frac{3}{2} P \psi_m i_q = K_t i_q \tag{3.16}$$

Where $K_t = \frac{3}{2} P \psi_m$ represents the torque constant.

$$T_{em} = T_l + J \frac{d}{dt} \omega_m + B \omega_m \tag{3.17}$$

Where J represents inertia, B is the coefficient of viscous friction, and T_l is the load torque.

3.5.2 Constant torque operation

The d axis current is only partially visible, but the q axis current is unmistakably the same as the dc machine's armature current. It supplies just a tiny amount of the field current; the matching current source, which mimics the permanent magnet field, provides the remaining portion [30].

$$i_d = I_s cos\alpha \tag{3.18}$$

$$i_q = I_s sin\alpha$$

where the torque angle is the angle formed between the rotor field and the stator's current phase. This leads to the angle being chosen to be 90 degrees, as shown in Figure 3.7. Equation (3.16) for electromagnetic torque can then be

$$T_{em} = K_t i_q = K_t I_s sin\alpha \tag{3.19}$$

The motor current determines the torque, much like a DC motor.

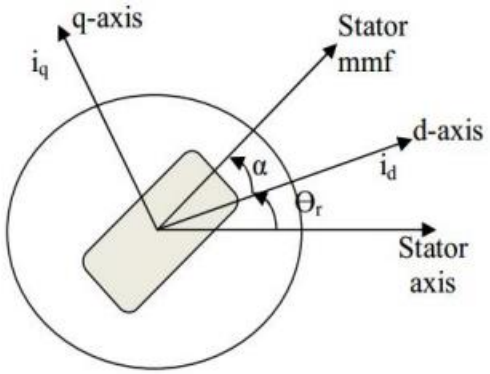

Figure 3.8: PMSM motor axes

To separately regulate the direct-axis stator current (a component that creates field) and the quadrature-axis stator current i q, the impacts of these coupling terms must be eliminated at the current PI controller's output (a component that produces torque). To utilize the stator voltage components from Equations (3.11) and, decoupling is necessary (3.12). The synchronous motor's terminal voltages are used to officially manage these stator current components since the stator voltage equations must be detached in order to regulate the stator currents i d and i q individually (decoupled control). [30].This serves solely to demonstrate that the system's non-linear component is overcome by the FOC controlling mechanism, therefore its impact is not taken into account during the simulation design phase. Currently, the d and q axis' decoupling voltage components are generated via the following formulae:

$$V_q D = \omega_{re} L_d i_d + \omega_{re} \psi_m \tag{3.20}$$

$$V_q D = \omega_r L_q i_q \tag{3.21}$$

3.6 General Control Scheme of PMSM Drive System

The different driving system components have been discussed and described in this section. The existing regulated VSI structure serves as the FOC's cornerstone. Variable or fixed output voltages and frequencies are both possible. If the input DC voltage is changed while the inverter's gain is constant, the output voltage will fluctuate.

On the other hand, the inverter's PWM control is often utilized to achieve this if the fixed DC input voltage cannot be changed.

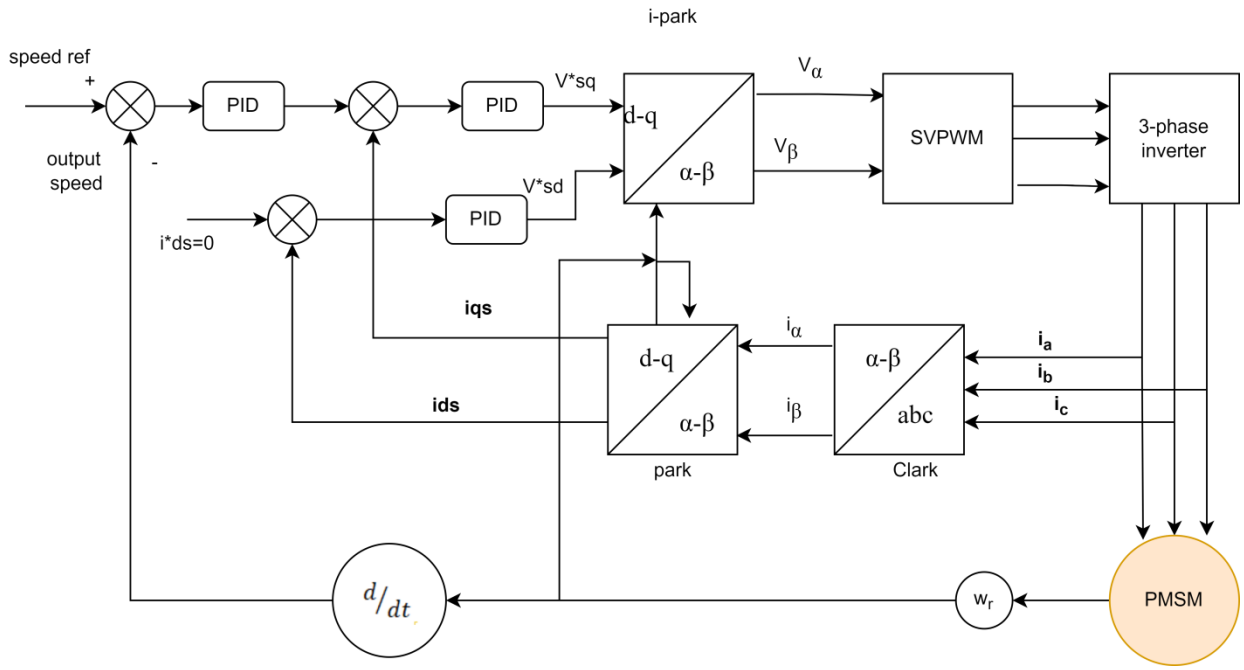

Figure 3.9:FOC of the PMSM drive mechanism

3.7 Three-phase PWM Voltage Source Inverter

Anti-parallel diodes and insulated gate bipolar transistors make up each power switch (IGBTs). When the top switch is engaged, the voltage on the poles or legs can increase to a value of + 0.5 V dc, and when the bottom switch is engaged, it can decrease to - 0.5 V dc. The symbols used to represent the phase voltage supplied to the load are V an, V bn, and V cn. In reality, a little dead band is supplied to ensure that the top and lower switches work in concert. [30] [25]. As seen in [25], leg voltage and switching signals have a connection;

$$V_k = Sk * Vdc; k = A, B, C \tag{3.22}$$

If the load is seen as a three-phase star arrangement, the relationship between the leg voltages and the phase-to-neutral load voltage is depicted as follows: [25]

$$VA(t) = va(t) + vnN(t) \tag{3.23}$$

$$VB(t) = vb(t) + vnN(t)$$

$$VC(t) = vc(t) + vnN(t)$$

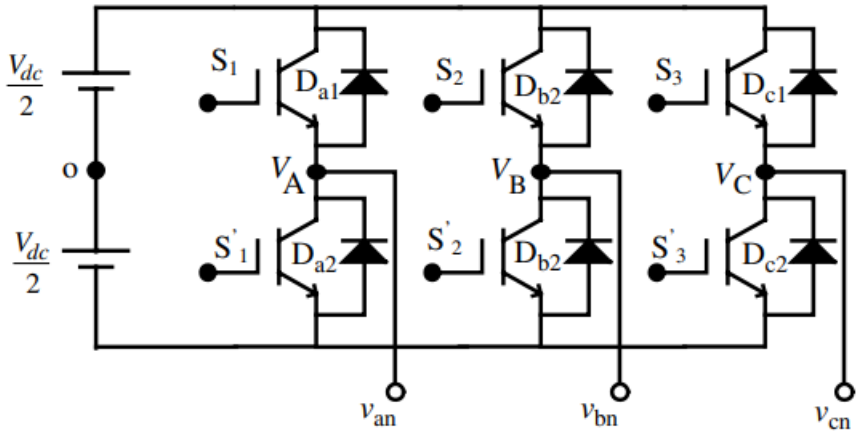

Figure 3.10: Topology of a three-phase VSI's power circuit [25]

A balanced three-phase voltage is assumed to have an immediate sum that is always zero. By summing each term in Equation (3.23) and putting the sum of phase to neutral voltage to zero, the following result is achieved [15]:

$$vnN(t) = \frac{1}{2}[VA(t) + VB(t) + VC(t)] \tag{3.24}$$

The phase-to-neutral voltage equations below are produced [15] by inserting Equation (3.24) again into Equation (3.23):

$$va(t) = \frac{2}{3}VA(t) - \frac{1}{3}[VB(t) + VC(t)] \tag{3.25}$$

$$vb(t) = \frac{2}{3}VB(t) - \frac{1}{3}[VA(t) + VC(t)]$$

$$vc(t) = \frac{2}{3}VC(t) - \frac{1}{3}[VB(t) + VA(t)]$$

Equation (3.22)'s formulation of the switching function could also be used to form Equation (3.25):

$$va(t) = \frac{1}{3}Vdc[2SA - SB - SC] \tag{3.26}$$

$$vb(t) = \frac{1}{3}Vdc[2SB - SA - SC]$$

$$vc(t) = \frac{1}{3}Vdc[4SC - SB - SA]$$

And Figure 3.10 displays the related waveforms for six-step modes.

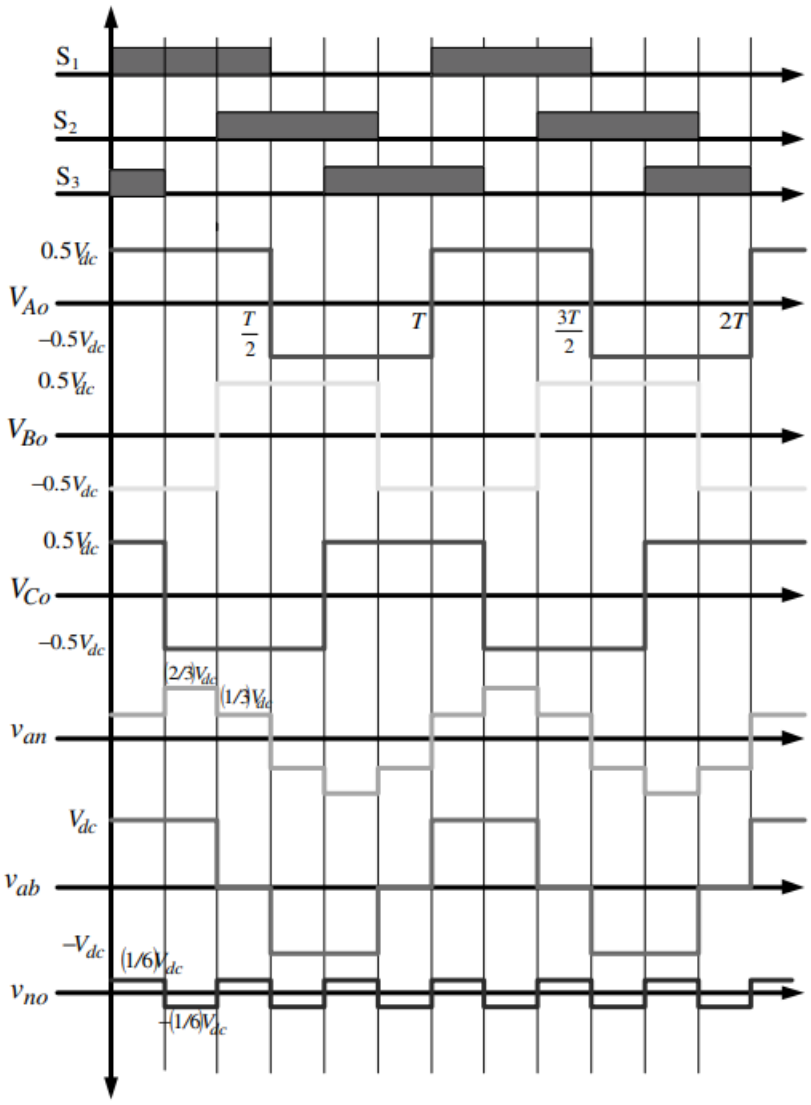

Figure 3.11: Waveforms for a three-phase inverter operating in square wave mode [25]

Table 3.1 lists the leg voltage levels for each of the inverter's six operational phases. Equation was used to compute the line voltages, which are displayed in Table 3.3.

$$vab = van - vbn \tag{3.27}$$

$$vbc = vbn - vcn$$

$$vca = vcn - van$$

Table 3.1: Voltages at the legs and poles of a three-phase VSI operating in six steps

Switching Mode	Switches ON	Leg voltage V_A	Leg voltage V_B	Leg voltage V_C
1	S_1, S_2', S_3	$0.5V_{dc}$	$-0.5V_{dc}$	$0.5V_{dc}$
2	S_1, S_2', S_3'	$0.5V_{dc}$	$-0.5V_{dc}$	$-0.5V_{dc}$
3	S_1, S_2, S_3'	$0.5V_{dc}$	$0.5V_{dc}$	$-0.5V_{dc}$
4	S_1', S_2, S_3'	$-0.5V_{dc}$	$0.5V_{dc}$	$-0.5V_{dc}$
5	S_1', S_2, S_3	$-0.5V_{dc}$	$0.5V_{dc}$	$0.5V_{dc}$
6	S_1', S_2', S_3	$-0.5V_{dc}$	$-0.5V_{dc}$	$0.5V_{dc}$

Table 3.2 : Voltages for a six-step operation's phase-to-neutral

Switching Mode	Switches ON	phase voltage v_{an}	phase voltage v_{bn}	phase voltage v_{cn}
1	S_1, S_2', S_3	$1/3V_{dc}$	$-2/3V_{dc}$	$1/3V_{dc}$
2	S_1, S_2', S_3'	$2/3V_{dc}$	$-1/3V_{dc}$	$-1/3V_{dc}$
3	S_1, S_2, S_3'	$1/3V_{dc}$	$1/3V_{dc}$	$-2/3V_{dc}$
4	S_1', S_2, S_3'	$-1/3V_{dc}$	$2/3V_{dc}$	$-1/3V_{dc}$
5	S_1', S_2, S_3	$-2/3V_{dc}$	$1/3V_{dc}$	$1/3V_{dc}$
6	S_1', S_2', S_3	$-1/3V_{dc}$	$-1/3V_{dc}$	$2/3V_{dc}$

The line-to-line voltage in the six-step mode is 1.1Vdc, and peak output phase-to-neutral voltage at its highest level is 0.6367Vdc or (2/3) Vdc.

Table 3.3: Line voltages for operation in six steps

Switching Mode	Switches ON	line voltage v_{ab}	phase voltage v_{bc}	phase voltage v_{ca}
1	S_1, S_2', S_3	V_{dc}	V_{dc}	0
2	S_1, S_2', S_3'	V_{dc}	0	V_{dc}
3	S_1, S_2, S_3'	0	V_{dc}	V_{dc}
4	S_1', S_2, S_3'	V_{dc}	V_{dc}	0
5	S_1', S_2, S_3	V_{dc}	0	V_{dc}
6	S_1', S_2', S_3	0	V_{dc}	V_{dc}

3.8 PWM Techniques

The use of various in-vector control approaches utilizing PWM techniques in AC motor drive applications is growing in popularity as a result of advancements in solid-state power electronic devices and microprocessors. The frequency and magnitude of the motor voltages are both controlled by such PWM-based systems. PWM technique is crucial for reducing switching losses and harmonics in converters, particularly in three-phase applications. Any modulation technique's primary goal is to produce a varied output with a maximum foundational element and a minimal harmonic content. These PWM method they include space vector PWM, third-harmonic PWM (THIPWM), and carrier-based PWM.SPWM stands for sinusoidal PWM. The Space Vector modulation approach is one of the most sophisticated and computationally costly PWM methods available, and it may be the best PWM method for driving applications [30], [31], [25].

3.8.1 Space Vectors Pulse Width Modulation (SVPWM)

This approaches because it employs a greater DC bus voltage (increased output voltage compared to SPWM). The inverter output must be expressed as space vectors or space phasors in order to comply with the SVPWM idea. A space vector representation of the inverter's output voltages is created in order to produce SVPWM.

A circle that depicts a sinusoidal function can be used to symbolize the state mapping. The linear modulation zone, also known as the under-modulation region, is the space inside the enclosing circle. The over- or nonlinear-modulation area is the region between the inner and outer circles of the hexagon, as shown in Figure 3.11 below. The modulation index affects how concepts in the linear and nonlinear modulation domains operate, which has an indirect effect on the inverter utilization capacity.

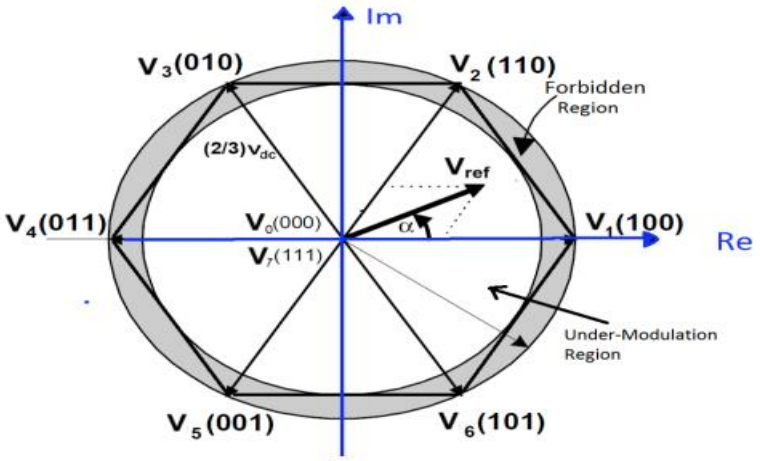

Figure 3.12: Space vector representation's under- and over-modulation regions [26]

By injecting third harmonics and lowering the demand for filter design, Max-Min offset is provided to lessen switching loss brought on by pure SVPWM. In order to resolve this issue, the max min offset method is utilized.

3.8.2 Principle and Implementation of Space Vector PWM

Six switches and eight different inverter configurations are used to regulate the three-phase inverter, as was mentioned on the preceding pages. You can convert the eight inverter states into their respective eight space vectors

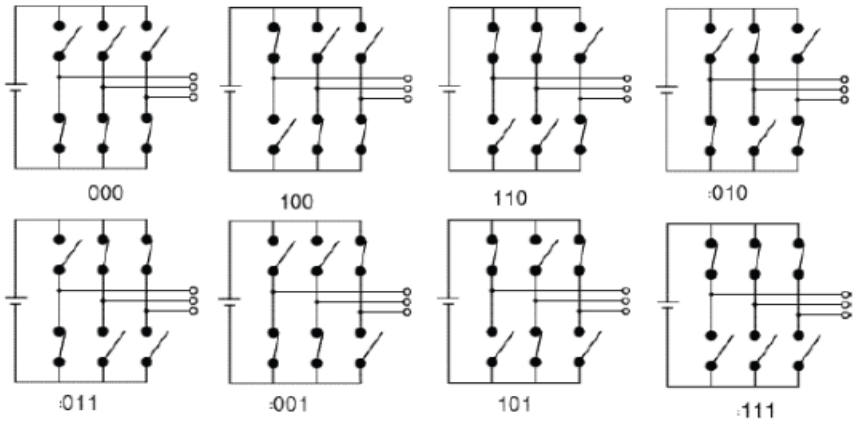

Figure 3-13:A three-phase inverter's eight switching states [13]

CHAPTER FOUR
CONTROLLER DESIGN OF PMSM

4.1 Introduction

PID controllers are commonly used in motor drive control systems. The standard PID controller, however, can't always maintain good performances since its settings are fixed while it is in use after being chosen using a certain optimal technique. The answer to this issue is to dynamically modify the controller's settings in response to the current operational status of the system. As a result, the self-tuning PID controller is examined in this chapter. Based on the error and the rate of change in the error, the PID controller settings are predicted using online fuzzy rules and reasoning. The rule bases are developed by researching an example step response and examining how modifications to the PID controller's parameter gains impact the system output.

4.2 PID Controller

Motor driving systems have frequently employed PID controllers. Over 90% of industrial controllers use PID algorithms in their implementation. PID controllers have a very straightforward construction and a very obvious control principle. It is useful and very simple to put into practice. Furthermore, the three PID controller components may be effectively tweaked to provide the necessary transient and steady-state responses because their functions are extremely obvious [34].

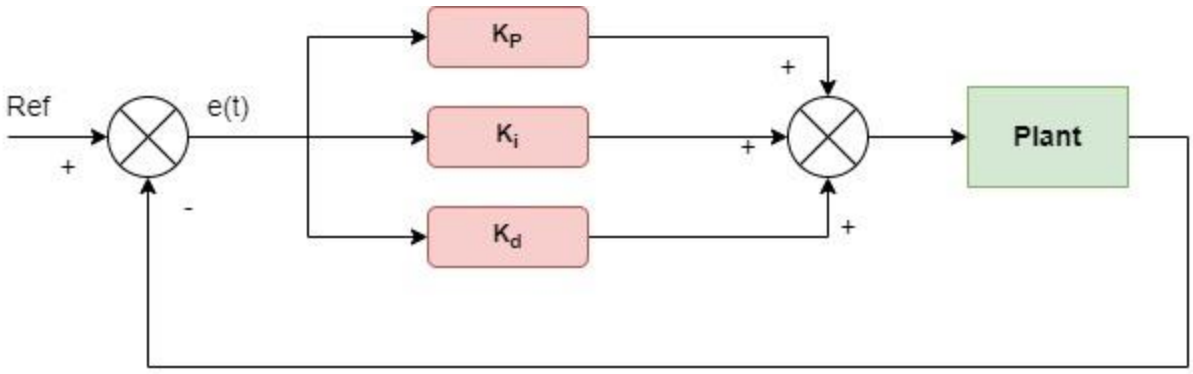

Figure 4.1: PID controller's block diagram

The following [31] is an example of a PID controller technique:

$$e(t) = r(t) - y(t) \tag{4.1}$$

$$u(t) = K_p e(t) + K_i \int e(t)dt + K_d \frac{de(t)}{dt} \tag{4.2}$$

$$(t) = K_p \left\{ e(t) + \frac{1}{T_i} \int e(t)dt + T_d \frac{de(t)}{dt} \right\} \tag{4.3}$$

Where y(t) stands for the system output, r(t) for the system's reference input, e(t) stands for the error signal between y(t) and r(t), and u(t) stands for the PID controller's output.

Equation (4.3)'s The Laplace transform is shown as follows:

$$U(s) = K_p \left(1 + \frac{1}{T_i s} + T_d s \right) \tag{4.4}$$

where K is integral gain, K_d is derivative gain, and K_p is the proportional gain T_i and T_d are integral and derivative time constants, respectively, and $K_i = \frac{K_p}{T_i}$, $K_d = K_p T_d$

4.3 FOPID controller

When integration and derivation order contain fractional values, a fractional order PID (PID) controller is an extension of a traditional PID controller. The system is made more adaptable and less sensitive by the updated controller with and commands for integral and derivative[35] . The differential formula could be used to describe the PI λDμ controller as:

$$u(t) = K_p e(t) + K_i D^{-\lambda} e(t) + K_d D^{\mu} e(t) \tag{4.5}$$

Whereas the following is how the Laplace transform can be used to illustrate the FOPID transfer function:

$$G(s) = K_p + K_i S^{-\lambda} + K_d S^{\mu} \tag{4.6}$$

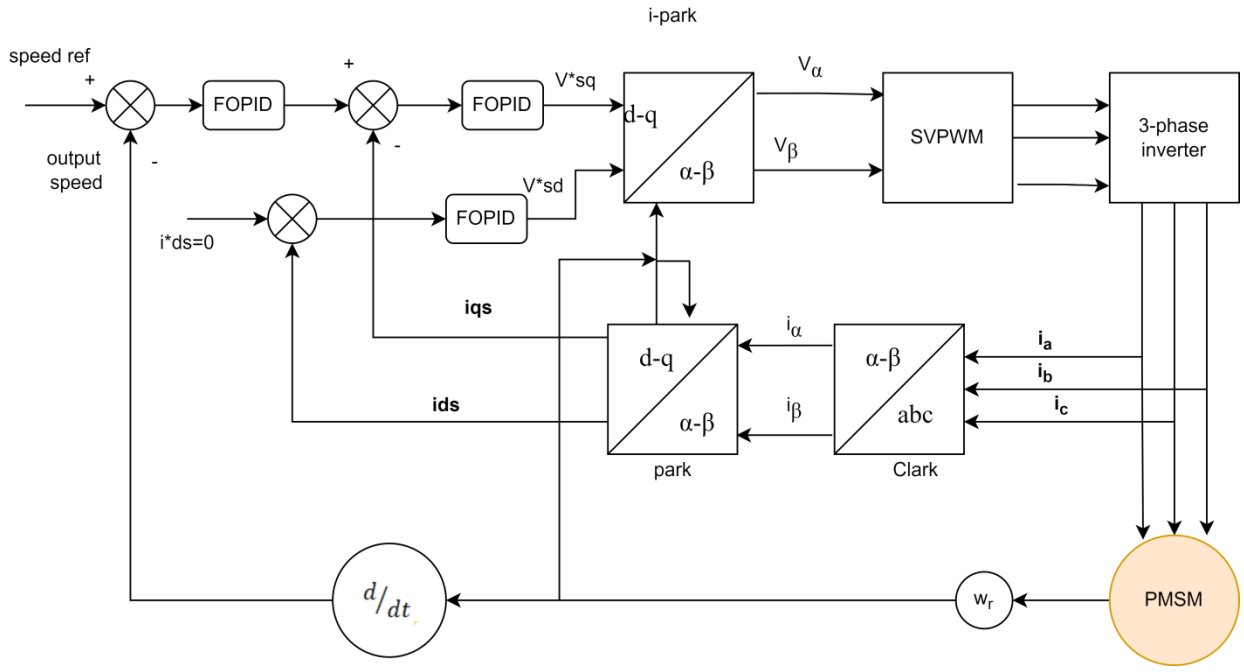

Figure 4.2: FOC strategy by FOPID controller

4.4 BACTERIAL FORAGING OPTIMIZATION ALGORITHM

The autonomous and cooperative foraging behavior of E. coli bacteria serves as the basis for BFO, a swarm intelligence-based numerical approach [36],[37]. It is inspired by nature. The bacteria tend to follow a path when seeking nutrients in order to get the most energy possible in a given amount of time. Exactly this attribute is used to address optimization issues. The fitness function used to characterize the optimization problem is the focus of the BFO algorithm, which aims to decrease its value [37],[38].

The following three bacterial foraging behaviors are simulated by the BFO algorithm:

- **Chemotaxis Process**

Chemotaxis is the name given to the mechanism by which bacteria use their flagella to both swim and tumble. When conditions are favorable, bacteria will continuously migrate in that direction whereas tumbling will cause them to change course. It aids in enhancing bacteria's ability to hunt globally.

The gain parameters of the PID controller, as it is being tuned, mimic the three axes of the three-dimensional search space. Equation indicates where the bacterium is located at the (j+1)th chemotaxis step, during the kth reproduction, and the elimination and dispersal phase (4.7).

$$P^{i,j+1,k,l}(K_p, K_i, K_d) = P^{i,j,k,l}(K_p, K_i, K_d) + c(i)\frac{\Delta(i)}{\sqrt{\Delta^T(i).\Delta(i)}} \quad (4.7)$$

Where c(i) stands for the chemotactic step size, I is a three-dimensional direction vector with each element standing for a value between [-1, 1], and T(i) stands for the transposition of the three-dimensional direction vector.

The bacteria continue to swim in the same direction if the fitness function's value at the (j+1)th step is lower than it was at the jth step; alternatively, if it is higher, I changes and the bacteria begin to sink.

- **Reproduction**

Healthy bacteria are able to live and reproduce in order to grow their population. but unhealthy bacteria ultimately kill according to nature's concept of survival of the fittest. The bacteria with the lowest fitness function values are split in half and placed in the same location to maintain population size while the bacteria with the highest fitness function values are eliminated to simulate this process artificially.

$$S_r = 0.5s$$

Where s is the size of the bacterial population and S_r is the number of bacteria that reproduce.

- **Elimination and Dispersal**

In the actual world, when the local environment of bacteria population changes due to water movement, temperature changes, or an increase in toxin levels, bacteria either die or spread to new areas. This activity, sometimes referred to as elimination and dispersal, exemplifies the bacteria's long-distance motile behavior. To simulate it, bacteria with probabilities of elimination and dispersal less than P_e are eliminated, and new bacteria are created at random locations

throughout the search space. This helps the bacteria search for global minimum solutions and prevents them from becoming caught in local minima.

The following is the BFO algorithm used to create an ideal PID speed controller for PMSM:

Step1: Set the BFO parameters $p, s,\ N_s, N_c,\ N_r, N_e,\ S_r, P_e,\ , \Delta, c(i))$ and preliminary values of $P^{i,j,k,l}\ (K_p, K_i, K_d)$ for $i = 1,2, \ldots s$.

Step 2: begin the loop for elimination and dispersion $l = l + 1$

Step 3: begin the reproductive cycle $k = k + 1$

Step 4: begin the chemotaxis cycle $j = j + 1$

The following describes a chemotactic process for i^{th} bacterium:

a) Determine the fitness function $J^{i,j,k.l}(K_p, K_i, K_d)$ using equation (4.9)
b) Maintain current fitness level $J_{last} = J^{i,j,k,l}(K_p, K_i, K_d)$ to look for more effective solutions.
c) Set (i) to a random number between [-1, 1] and then perform a tumble operation the use of equation (4.7) to get the microorganisms to tumble. The new fitness function $J^{i,j,k,l}(K_p, K_i, K_d)$ should be calculated.
d) execute a swim procedure
    i) start the swim counter m = 0; while m < Ns
    ii) If $J_{last} > J^{i,j,k,l}(K_p, K_i, K_d)$ keep swimming in the same direction.
    iii) A swim cycle will end if m = Ns is not set.
e) For each bacteria, repeat steps (a) through (d) until i = s.

Step 5: Carry out step 4 again until j=N c.

Step 6: Perform the following reproduction procedure:

a) Calculate the health of each bacteria for the provided k and l. $i = 1,2, \ldots s$

$$J_{health}^{i} = \sum_{j=1}^{N_c} J^{i,j,k,l}(K_p, K_i, K_d) \tag{4.8}$$

The S_r number of microorganisms with the highest value of J health is destroyed, while the S_r number of microorganisms with the lowest value of J_{health} are divided in half and placed in the same location.

Step 7: Up till$k = N_r$, repeat this step 4-6.

Step 8: Execute the following elimination and dispersion operation:

a) To keep population sizes constant, bacteria with elimination and dispersal probabilities less than P_e are eliminated and distributed randomly at a new place.

Step 8: Follow steps 3 through 8 until $1 = N_e$. Finish when 1=N e.

Figure 4.3 uses a flow chart to show the BFO algorithm.

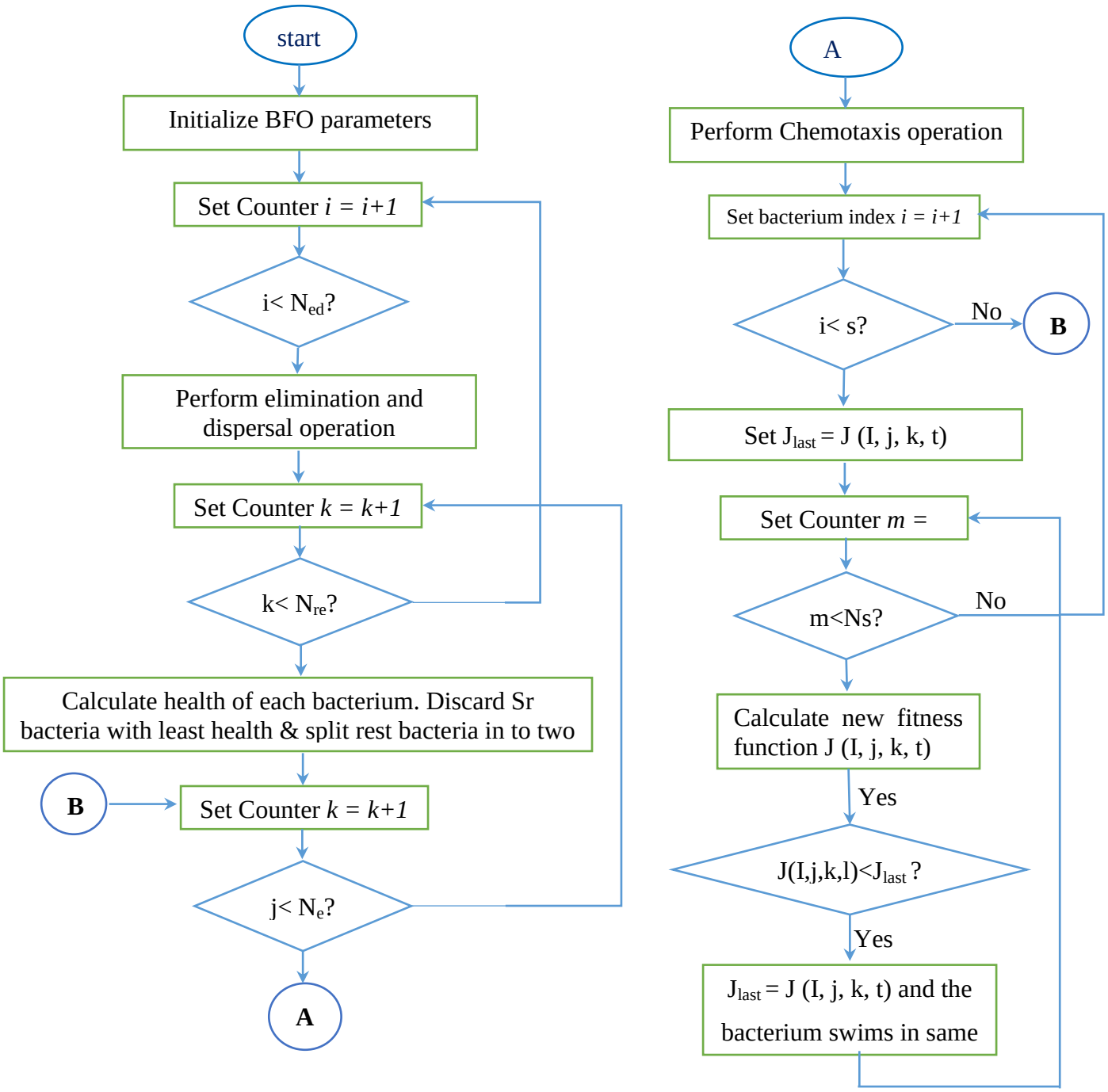

Figure 4.3: Flowcharts for BFO Algorithm

4.5 BFO-optimized PID control design

In this section, the system is optimized for the PID controller gains *Kp*, *Ki*, and K_p, K_i, K_d using the bacterial foraging optimization method. Figure 4.4 depicts the tuning of the BF-PID controller.

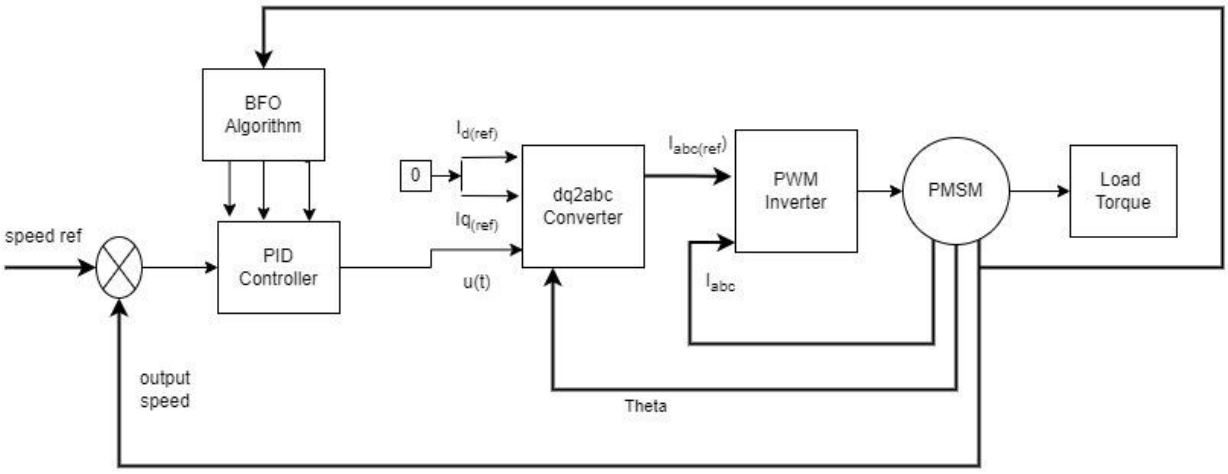

Figure 4.4: Block Diagram of the PMSM's PID Control System

4.5 FOPID CONTROLLERS DESIGN USING BFO

This section uses the bacterial foraging optimization method to enhance the PID controller gains $K_p, K_i, K_d, \mu \ and \ \lambda$. Tuning for the BF-FOPID controller is shown in Figure 4.5.

A set of PID and FOPID parameters must be specified in BF-based optimization in order to reduce the performance indication.

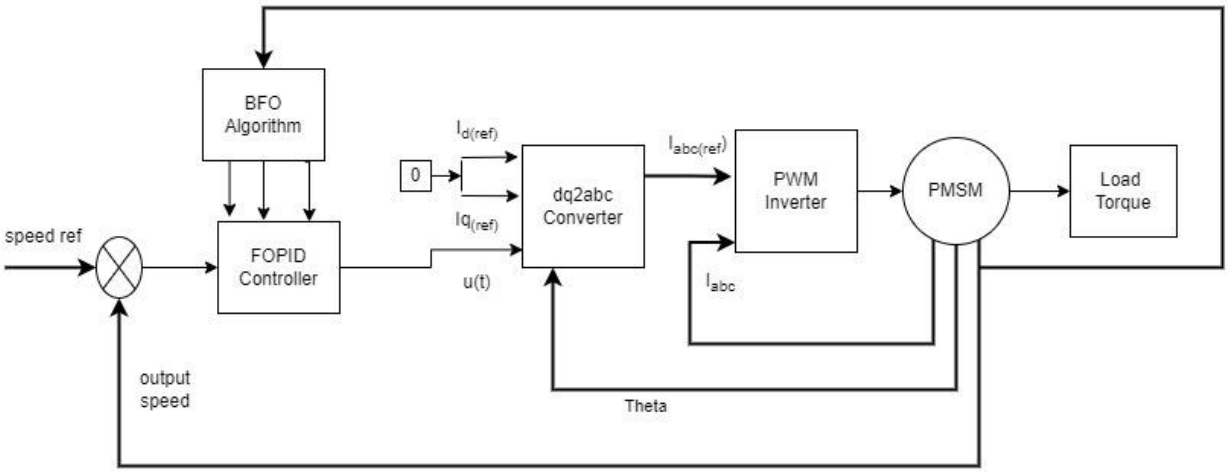

Figure 4.5:The BF-FOPID controller tuning

CHAPTER FIVE
SIMULATION RESULT AND DISCUSSION

The simulator for PMSM speed control was built using MatLab/Simulink and PID and FOPID controllers that were tuned using the Bacterial Foraging Optimization (BFO) method. The gain coefficients (proportional, integral, derivative, lambda *(ℷ)*, and(μ) of the PID speed controller and the (proportional, integral, derivative, and lambda (ℷ), and(μ) Fractional Order PID speed controller have been optimized using the Bacterial Foraging Optimization (BFO) approach. The PMSM component and parameter specifications shown in Table 5 1 were taken into account for this work in [37].

Table 5.1 Performance of speed control for PMSM using PID Controller

Variable	Parameters	Value	Units
R_d	Resistance to Stators	2.875	Ω
L_d	Axis-d inductance	1.53	Mh
L_q	inductance on the q-axis	1.53	Mh
λ_{af}	Linkage of permanent magnets with constant flux	0.175	Wb or V.s
J	kinetic energy	0.0008	Kg.m^2
P	Quantity of pole pairs	4	no

5.1 Performance of speed control for PMSM using PID Controller

Figure 5.1 displays the general Matlab/Simulink model of the PMSM drive and Control system for PID controller

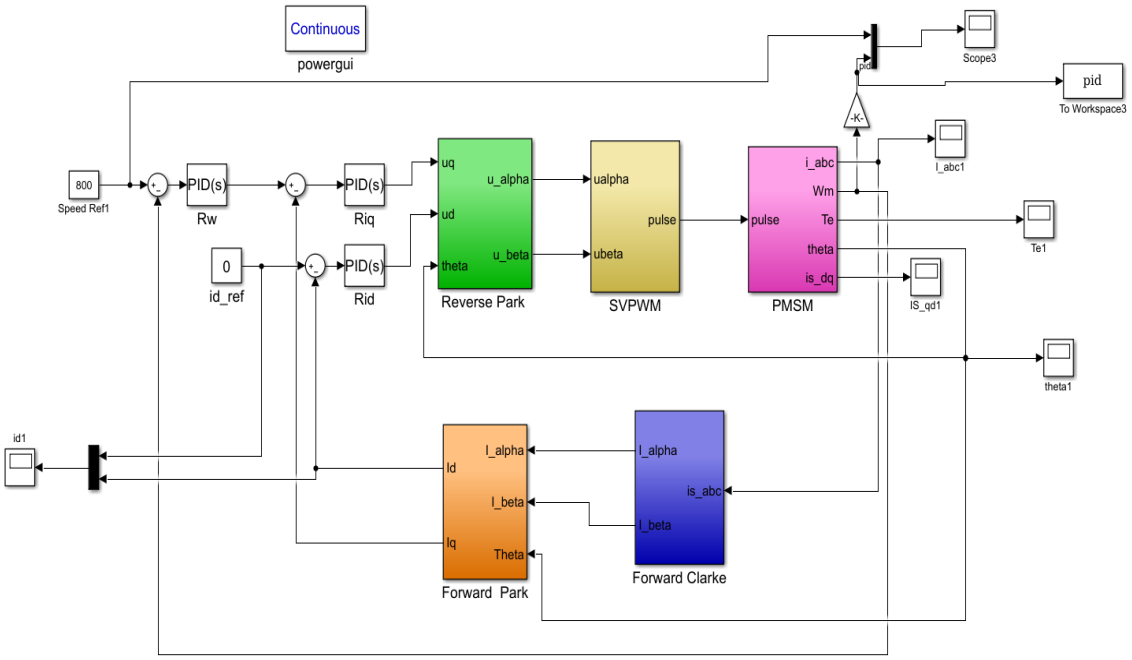

Figure 5.1:Simulink block diagram of PMSM by using PID controller

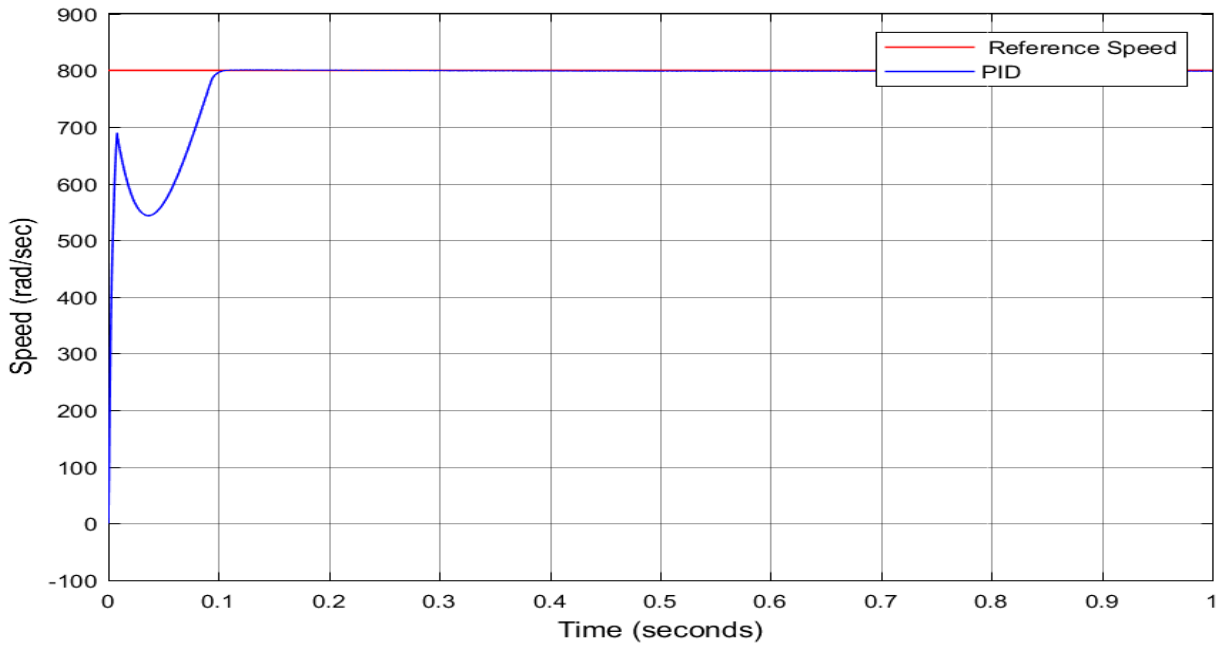

Figure 5.2: Speed response of motor for the PID controllers at constant speed of 800rad/sec

The above figure illustrates how the motor speed changes over time. The reference speed that is required and the steady state speed are identical. The system can follow the reference signal with a rising time of less than 0.082 seconds, a settling time of 0.094 seconds, and a maximum over shoot value of 0.368%, which shows that the system has acceptable transient and steady state response.

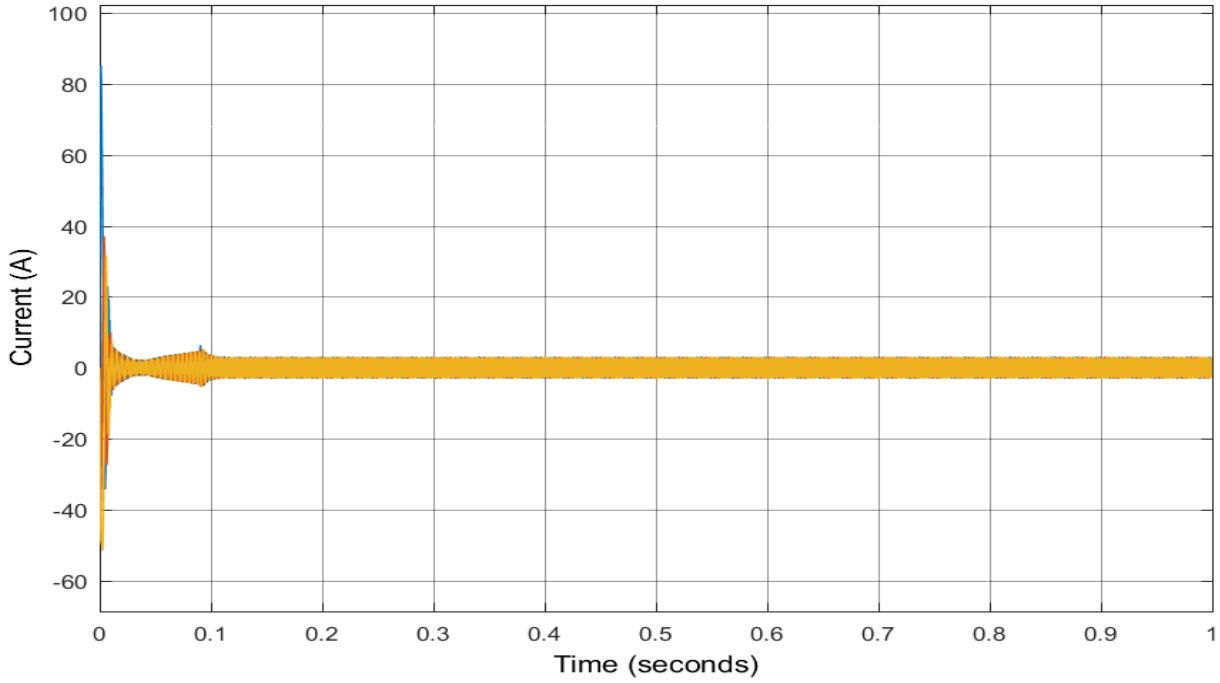

Figure 5.3:abc current response

It is obvious that the current is no sinusoidal at startup and sinusoidal once the motor has reached the controller's specified speed at steady state. The motor's two phase currents ($i_a, i_b \; and \; i_c$), as drawn by the motor when it is running at a reference speed, are shown in Figure 5.3.

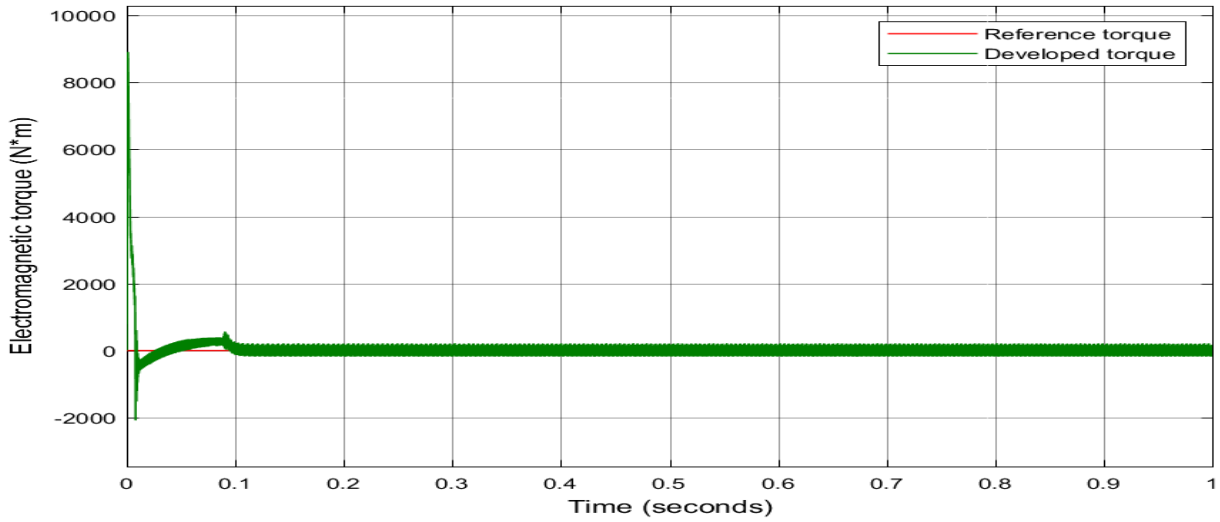

Figure 5.4: Developed electromagnetic torque.

The motor's produced electromagnetic torque under no load conditions is shown in Figure 5.4. The acceleration of the rotor to attain the stable speed of 800 rad/sec causes the variation in the starting torque that lasts for 0.09 seconds. In comparison to the steady state measurement, the startup torque is higher at 8500 Nm. However, the generated torque is practically decreased to zero Nm after 0.09 seconds in order to sustain only the essentially zero retard friction.

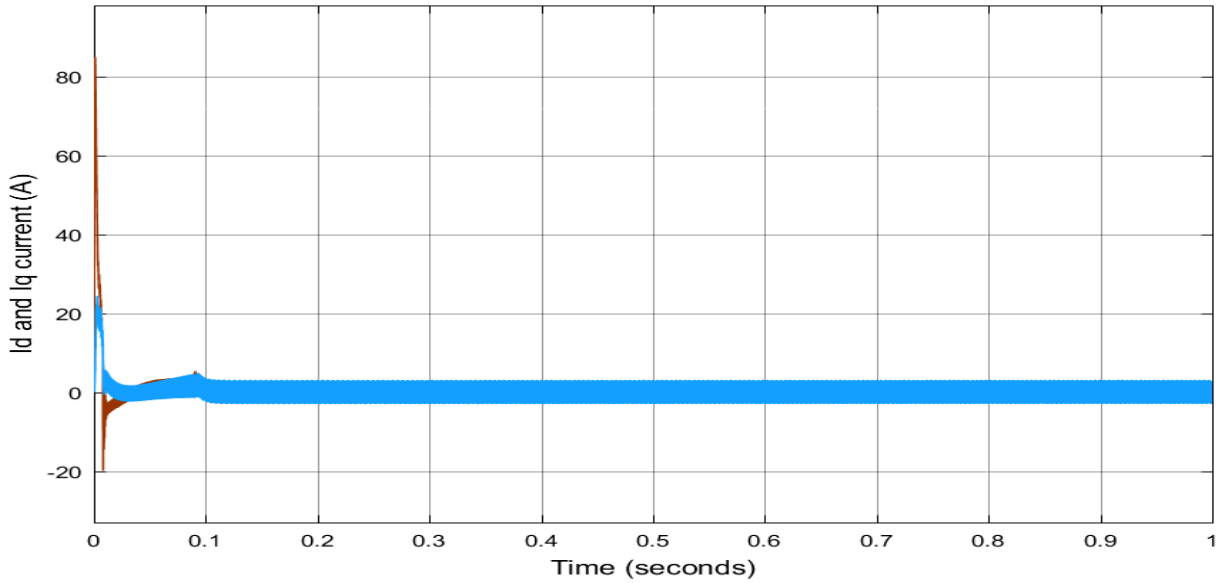

Figure 5.5:Is_dq response

5.2 Performance of speed control for PMSM using FOPID Controller

Figure 5.6 displays the general Matlab/Simulink model of the PMSM drive and Control system for PID controller. Every element of the real drive system is represented in order to analyze the simulation findings.

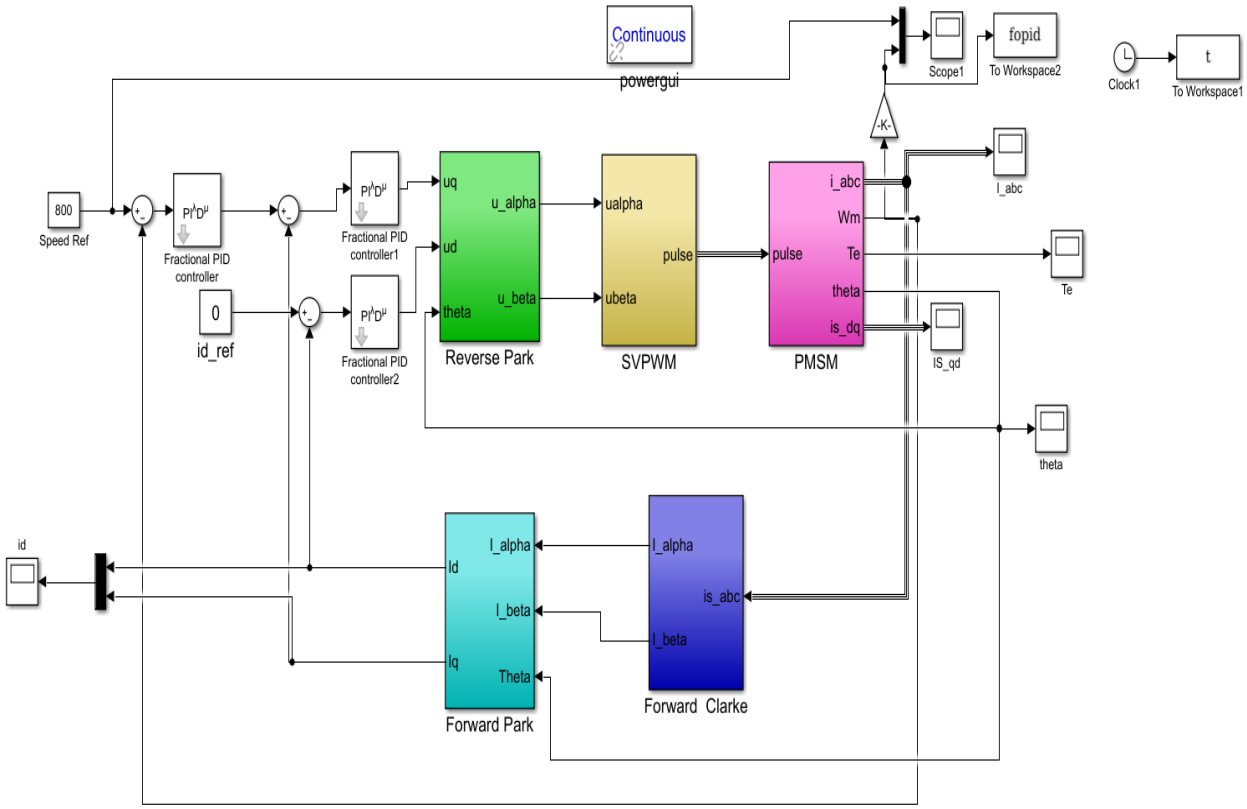

Figure 5.6:Simulink block diagram of PMSM by using FOPID controller

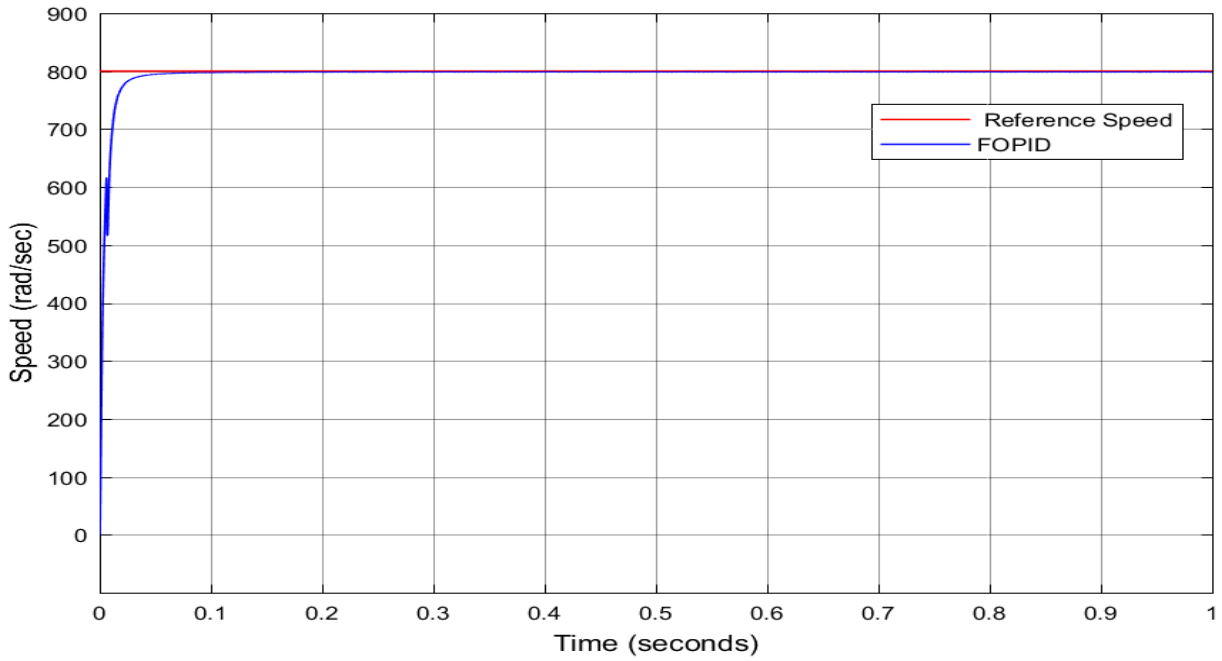

Figure 5.7: 800rad/sec is the FOPID controllers' speed reaction time

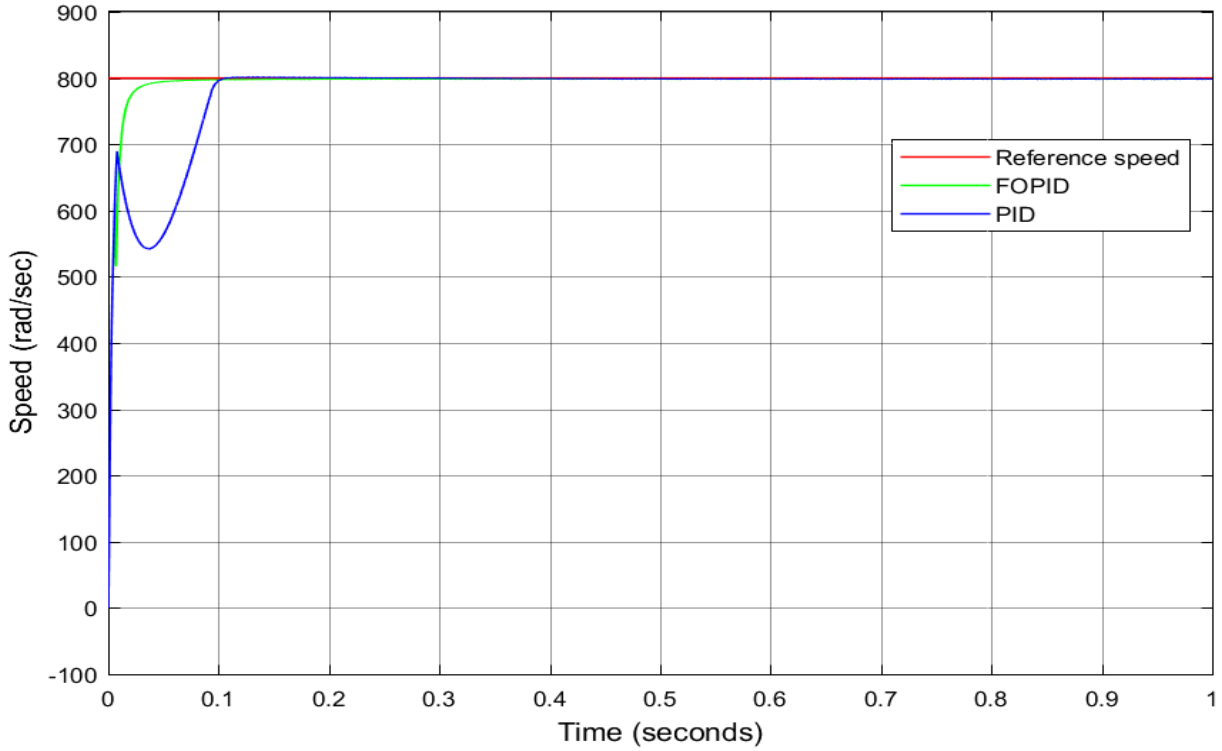

Figure 5.8: No load test for both controllers at 800 rad/sec

Tests with load

when a steady speed and a 2 Nm load torque are applied at t=0.2 seconds

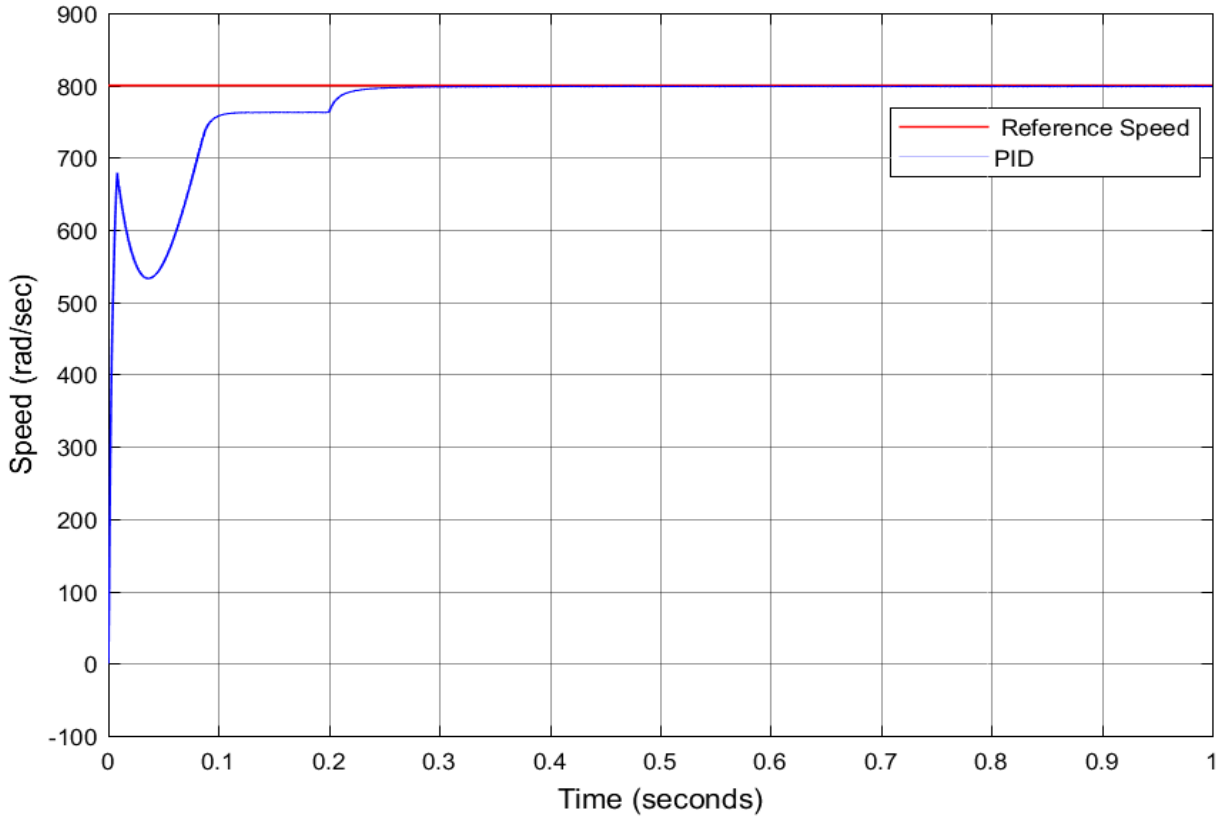

Figure 5.9: PID controller speed responses at 800 rad/sec with a 2 Nm load torque

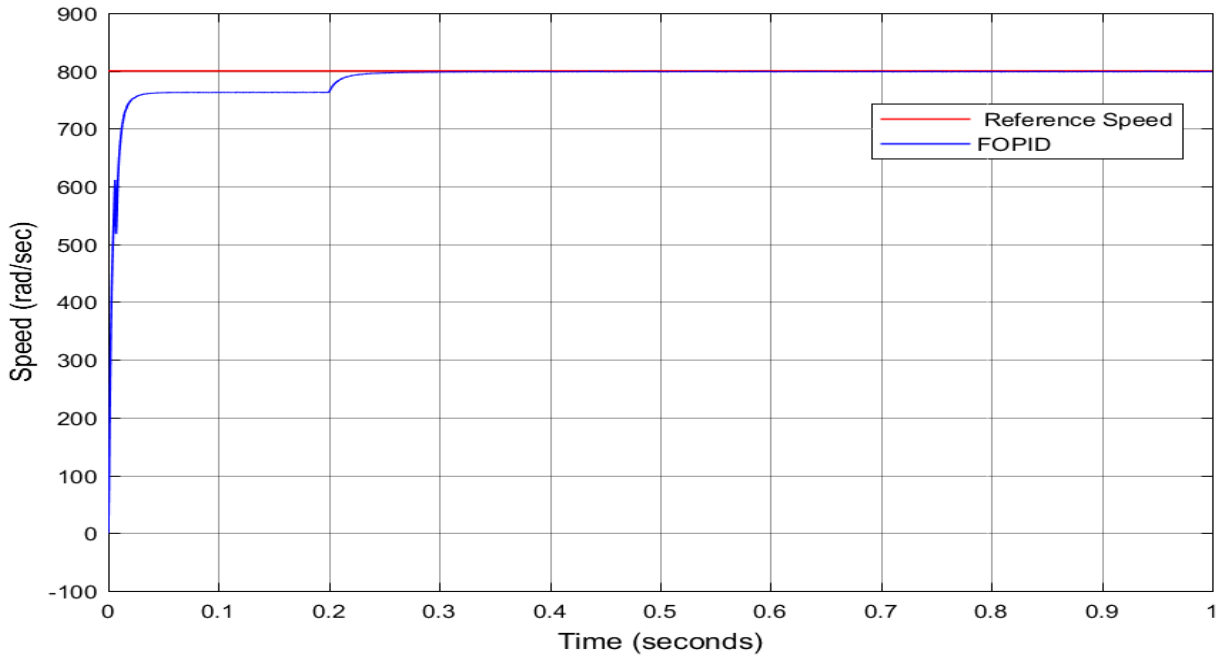

Figure 5.10: FOPID controllers' speed response is 800rad/sec with a 2 Nm load toque.

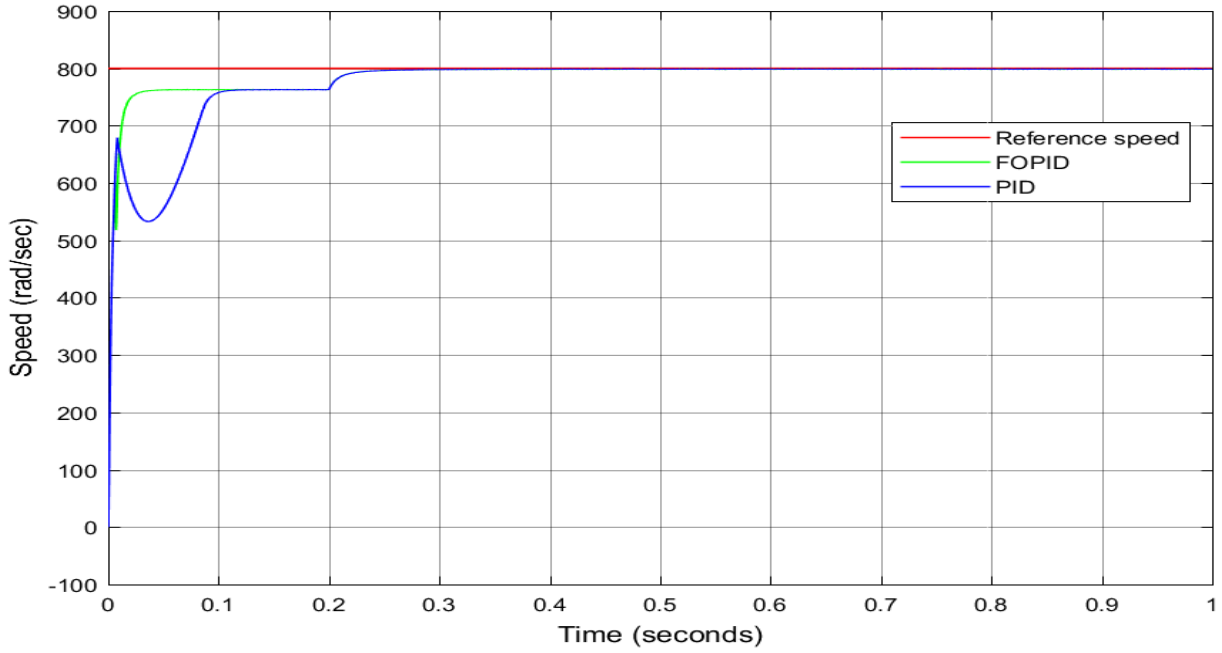

Figure 5.11: 800 rad/sec with a 2 Nm load toque is the speed response for the PID and FOPID controllers.

As shown in Figure 5.11, this test involves testing the proposed system with a 2Nm applied load torque at a time constant of 0.2 seconds. This test uses both PID and FOPID controllers, As compared to the no-load test, the % steady state inaccuracy is somewhat greater.

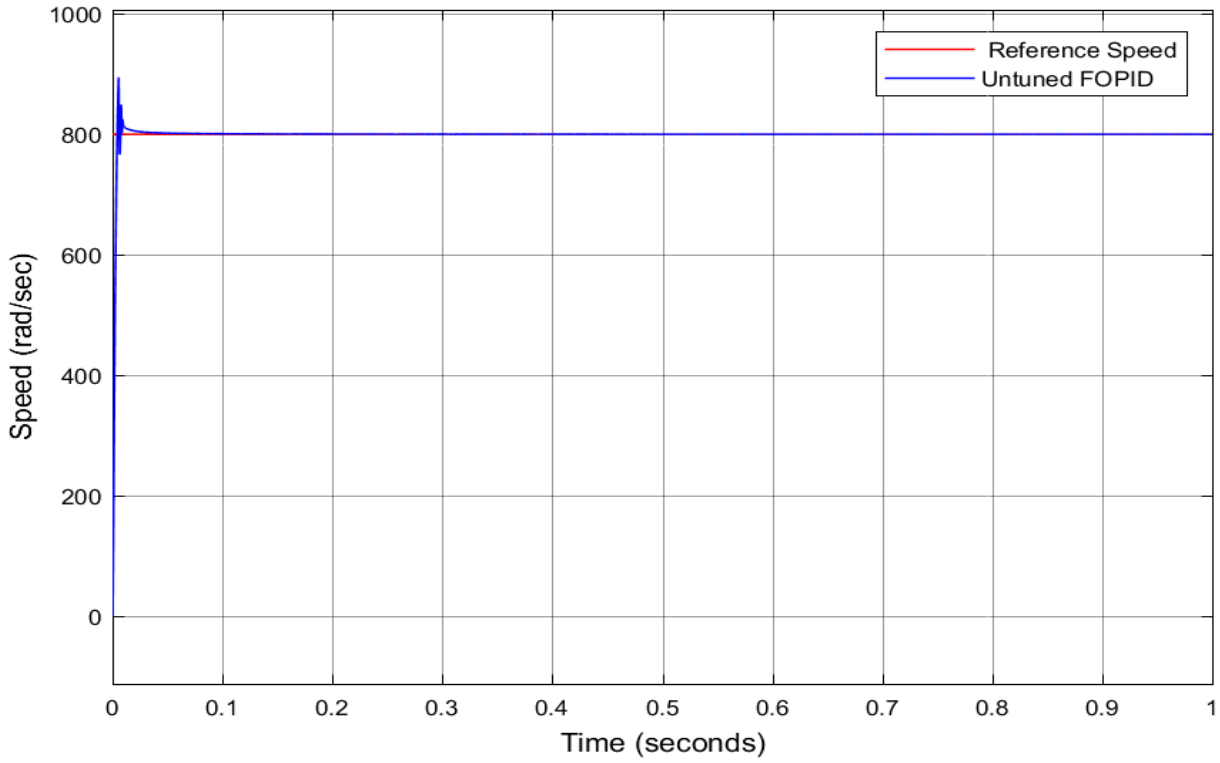

Figure 5.12: 800rad/sec is the unturned FOPID controllers' speed reaction time

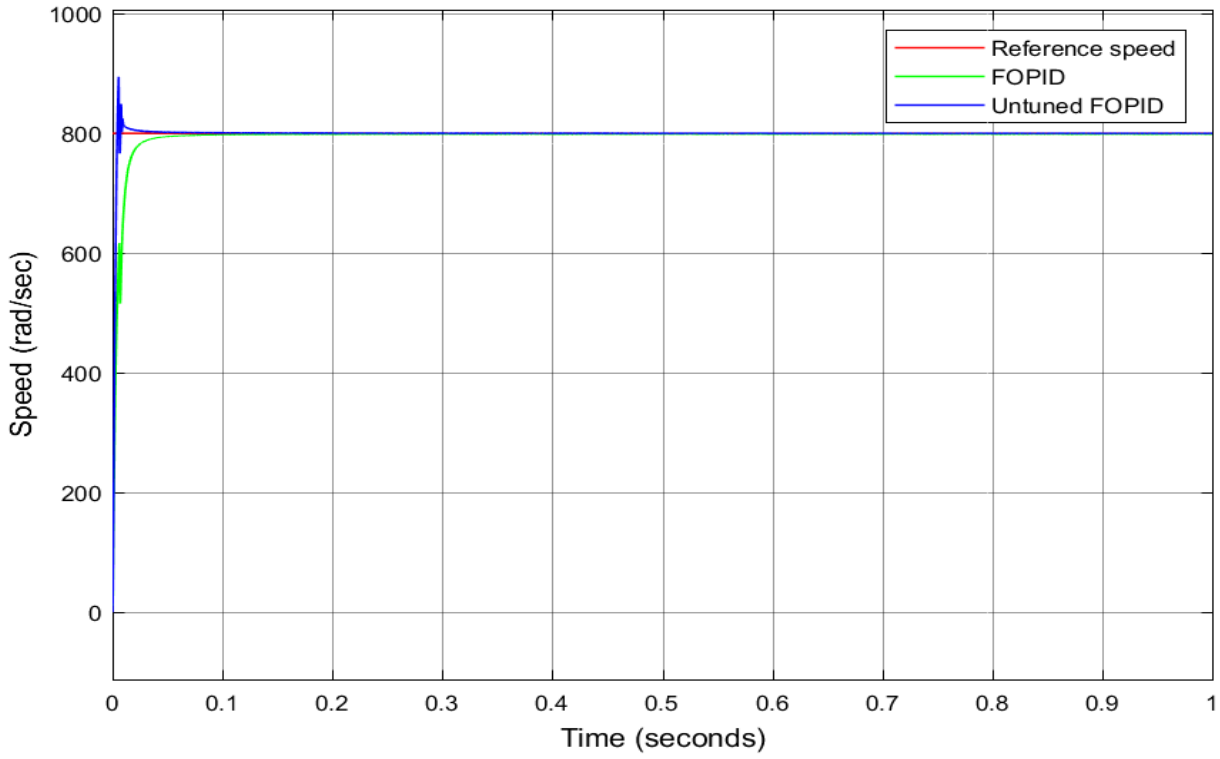

Figure 5.13: 800rad/sec is the tuned and unturned FOPID controllers' speed reaction time

5.3 Performance comparison of the FOPID controller and PID Controllers with BFO tuning

The simulation findings and discussions discussed above employ the system reactions to evaluate stability and performance. Table 5.2 below compares many metrics, such as overshoot, rising time, and settling time. Figures 5.8 and 5.11 display the output graphs of controllers with and without load.

Table 5.1:Time response comparison of PID and FOPID controller with BFO tuning

Test	Performance parameters	PID_BFO	FOPID_BFO
Without load torque	Settling time	0.0935	0.0256
	Rise time	0.0818	0.0118
	Over shoot	0.3680	0.043
When the load torque is 2Nm at t=0.2sec	Settling time	0.2083	0.2079
	Rise time	0.0834	0.0132
	Over shoot	0.0670	0.0648

To enable an examination of the findings, Table 5.1 compares the transient responses for both controllers, including rising time, settling time, and overshoot. In terms of rising time, settling time, and overshoot with regard to speed control of PMSM, the BFO based FOPID controller outperformed the BFO based PID controller. With no load, the FOPID controller's system characteristics are as follows: settling time: 0.0935 seconds; rise time: 0.0818 seconds; overshoot: 0.3680%; compared to the PID controller's 0.0256 seconds, 0.0118 seconds, and 0.043%.

CHAPTER SIX
CONCLUSION AND RECOMMENDATIONS

6.1 CONCLUSION

The primary focus of this thesis is on utilizing MATLAB/Simulink to manage the speed of a PMSM drive system using a BFO optimization PID and FOPID controller. The performances of various controllers are contrasted. The simulation outcomes for each controller are shown and reviewed. Findings from PID and FOPID speed controllers adjusted using BFO approaches have also been compared in order to evaluate the efficacy of each methodology. The transient speed response characteristics of the PMSM drive under load and no-load conditions were compared. Transient response parameters such as rising time (*tr*), settling time (*ts*), and maximum overshoot have been used to assess the drive's performance (*Mp*).

When comparing the settling times , rise times and overshot of the speed control of PMSM for the PID and the FOPID controller based BFO tuning, the FOPID controller has fewer settling times, rise times, and overshoot. It can be seen that the FOPID controller significantly increased the system's efficiency and performance.

6.2 Recommendation

This thesis only operates in the base speed region. It is thus recommended that the thesis be expanded to cover using the motor above its rated speed or in the area of the field's weakening. When the motor speed to be extended past base speed, a flux-weakening technique is used.

Recommendations for future works are listed as follows:

- To increase the system's effectiveness, an online parameter identification procedure should be used.
- Setting up an experiment and assessing the results in the lab.

REFERANCE

[1]J. Chen, W. Yao, Y. Ren, R. Wang, L. Zhang, en L. Jiang, "Nonlinear adaptive speed control of a permanent magnet synchronous motor", Control Eng. Pract., vol 85, bll 163–175, 2019

[2]N. V. Ramana en V. L. N. Sastry, "A Novel Speed Control Strategy for Five Phases Permanent Magnet Synchronous Motor with Linear Quadratic Regulator", Int. J. Comput. Electr. Eng., vol 7, no 6, bll 408–416, 2015

[3]J. I. Itoh, N. Nomura, en H. Ohsawa, "A comparison between V/f control and position-sensorless vector control for the permanent magnet synchronous motor", Proc. Power Convers. Conf. 2002, PCC-Osaka 2002, vol 3, bll 1310–1315, 2002

[4] Jacob.B.Rolng,C. Jensen, "Modelling and design of PMSM position drives using model following control", Handledare Bengt Erikson 2021.

[5] A. M. Nazelan, M. K. Osman, A. A. A. Samat, en N. A. Salim, "PSO-Based PI Controller for Speed Sensorless Control of PMSM", J. Phys. Conf. Ser., vol 1019.

[6] J. W. Jung, V. Q. Leu, T. D. Do, E. K. Kim, en H. H. Choi, "Adaptive PID speed control design for permanent magnet synchronous motor drives", IEEE Trans. Power Electron., vol 30, no 2, bll 900–908, 2015, doi: 10.1109/TPEL.2014.2311462.

[7] P. Pillay en R. Krishnan, "Control Characteristics and Speed Controller Design for a High Performance Permanent Magnet Synchronous Motor Drive", IEEE Trans. Power Electron., vol 5, no 2, bll 151–159, 1990, doi: 10.1109/63.53152.

[8] C. Q. Zhong, L. Wang, en C. F. Xu, "Path tracking of permanent magnet synchronous motor using fractional order fuzzy pid controller", Symmetry (Basel)., vol 13, no 7, 2021, doi: 10.3390/sym13071118.

[9] P. Gao, G. Zhang, H. Ouyang, en L. Mei, "An Adaptive Super Twisting Nonlinear Fractional Order PID Sliding Mode Control of Permanent Magnet Synchronous Motor

Speed Regulation System Based on Extended State Observer", IEEE Access, vol 8, bll 53498–53510, 2020, doi: 10.1109/ACCESS.2020.2980390.

[10] S. Tehsin et al., "Self-Organizing Hierarchical Particle Swarm Optimization of Correlation Filters for Object Recognition", IEEE Access, vol 5, bll 24495–24502, 2017, doi: 10.1109/ACCESS.2017.2762354.

[11] Y. Shi, "Field Oriented Control of Permanent Magnet Synchronous Motor With Third-Harmonic Injection Pulse Width Modulation To Reduce Quadrotors' Speed Ripples", New Jersey Inst. Technol., bl 63, 2017.

[12] P. P. Acarnley en J. F. Watson, "Review of position-sensorless operation of brushless permanent-magnet machines", IEEE Trans. Ind. Electron., vol 53, no 2, bll 352–362, 2006, doi: 10.1109/TIE.2006.870868.

[13] K. Zhou en D. Wang, "Relationship between space-vector modulation and three-phase carrier-based PWM: A comprehensive analysis", IEEE Trans. Ind. Electron., vol 49, no 1, bll 186–196, 2002, doi: 10.1109/41.982262.

[14] S. Sachan, S. Saway, en A. Singhal, "Simulation of Three Phase Voltage Source Inverter Based on SVPWM Technique", no June 2021, bll 141–146, 2018, doi: 10.1007/978-3-319-63085-4_19.

[15] M. B. B. Sharifian, T. Herizchi, en K. G. Firouzjah, "Field oriented control of permanent magnet synchronous motor using predictive space vector modulation", 2009 IEEE Symp. Ind. Electron. Appl. ISIEA 2009 - Proc., vol 2, no Isiea, bll 574–579, 2009, doi: 10.1109/ISIEA.2009.5356385.

[16] K. Jash, P. Pradip, K. Saha, P. Goutam, en K. Panda, "Vector control of permanent magnet synchronous motor based on sinusoidal pulse width modulated inverter with proportional integral controller", Int. J. Eng. Res. Appl., vol 3, no 5, bll 913–917, 2013.

[17] E. P. Engineering, "Speed Controller Design of Permanent Magnet Synchronous Motor

used in Washing Machine", vol 03, no 15, bll 3212–3217, 2014.

[18] X. Liu, "Control Strategy of Rare Earth Permanent Magnet Synchronous Motor", J. Phys. Conf. Ser., vol 2218, no 1, bll 0–3, 2022, doi: 10.1088/1742-6596/2218/1/012061.

[19] P. L. Chapman, "Permanent-magnet synchronous machine drives", Power Electron. Handb. Ind. Electron. Ser., bll 12-1-12–10, 2001, doi: 10.1002/9781119260479.ch9.

[20] S. Bassi, E. Gbenga, A. Abidemi, D. Opeoluwa, en B. Mohammed, "Heliyon Metaheuristic algorithms for PID controller parameters tuning : review , approaches and open problems", Heliyon, vol 8, no May, bl e09399, 2022, doi: 10.1016/j.heliyon.2022.e09399.

[21] C. Knospe, "PID control", IEEE Control Syst., vol 26, no 1, bll 30–31, 2006, doi: 10.1109/MCS.2006.1580151.

[22] G. Grandi, A. Tani, P. Sanjeevikumar, en D. Ostojic, "Multi-Phase Multi-Level AC Motor Drive Based on Four Three-Phase Two-Level Inverters", bll 1768–1775, 2010.

[23] C. I. Muresan, I. Birs, C. Ionescu, en E. H. Dulf, "A Review of Recent Developments in Autotuning Methods for Fractional-Order Controllers", 2022.

[24] High Performance Control of Ac Drives With Matlab / Simulink Models High Performance Control of Ac Drives With Matlab / Simulink. .

[25] P. Sala-Perez, S. Galceran-Arellano, en D. Montesinos-Miracle, "A sensorless stable V/f control method for a five-phase PMSM", 2013 15th Eur. Conf. Power Electron. Appl. EPE 2013, 2013, doi: 10.1109/EPE.2013.6631943.

[26] H. Teshager, "Design and Simulation of Speed Control of PMSM with Fuzzy Logic Self-Tuning PID Controller using MATLAB", no March, bll 1–32, 2017.

[27] C. Busca, "Open Loop Low Speed Control for PMSM in High Dynamic Applications", bl 119, 2010.

[28] T. Instruments, "Field orientated control of 3-phase AC-motors", Lit. number BPRA073, 1998.

[29] Mahlet Legesse Gebresilassie, "Speed Control of Vector Controlled PMSM Drive using Fuzzy Logic-PI Controller", thesis for the degree of Master of Science in Electrical and Computer Engineering Addis Ababa Institute of Technology (AAiT) ,August, 2011

[30] N. Xuan-Mung en S. K. Hong, "Improved altitude control algorithm for quadcopter unmanned aerial vehicles", Appl. Sci., vol 9, no 10, 2019, doi: 10.3390/app9102122.

[31] A. Mishra and P. Choudhary, "Speed control of an induction motor by using indirect vector control method," Int. J. Emerg. Technol. Adv. Eng., vol. 2, no. 12, pp. 144–150, 2012.

[32] I. Husain, "Electric Motor Drives", Electric and Hybrid Vehicles. bll 309–358, 2020, doi: 10.1201/9781439894972-12.

[33] J. Holtz, W. Lotzkat, en A. M. Khambadkone, "On Continuous Control of PWM Inverters in the Overmodulation Range Including the Six-Step Mode", IEEE Trans. Power Electron., vol 8, no 4, bll 546–553, 1993, doi: 10.1109/63.261026.

[34] M. Vagia, PID Controller Design Approaches: Theory, Tuning and Application to Frontier Areas. BoD--Books on Demand, 2012.

[35] Y. S. Mezaal, H. T. Eyyuboglu, en J. K. Ali, "A novel design of two loosely coupled bandpass filters based on hilbert-zz resonator with higher harmonic suppression", Int. Conf. Adv. Comput. Commun. Technol. ACCT, bll 343–347, 2013, doi: 10.1109/ACCT.2013.54.

[36] K. M. Passino, "Biomimicry of Bacterial Foraging for Distributed Optimization and Control", IEEE Control Syst., vol 22, no 3, bll 52–67, 2002, doi: 10.1109/MCS.2002.1004010.

[37] *S. Agarwal, D. Yadav, en A. Verma, "Speed control of PMSM drive using bacterial foraging optimization", 2017 4th IEEE Uttar Pradesh Sect. Int. Conf. Electr. Comput. Electron. UPCON 2017, vol 2018-January, bll 84–90, 2017, doi: 10.1109/UPCON.2017.8251027.*

[38] *G. Wu, "Application of adaptive PID controller based on bacterial foraging optimization algorithm", 2013 25th Chinese Control Decis. Conf. CCDC 2013, bll 2353–2356, 2013, doi: 10.1109/CCDC.2013.6561331.*